AN AERODYNAMIC TRADEOFF STUDY OF THE SCISSOR WING CONFIGURATION

BRUCE P. SELBERG

KAMRAN ROKHSAZ

CLINTON S. HOUSH

UNIVERSITY OF MISSOURI-ROLLA

MECHANICAL ENGINEERING & AEROSPACE ENGINEERING

& ENGINEERING MECHANICS DEPARTMENT

ROLLA, MO 65401

GRANT NAG-1-975

MAY 1990

AN AERODYNAMIC TRADEOFF STUDY OF THE SCISSOR WING CONFIGURATION

BRUCE P. SELBERG

KAMRAN ROKHSAZ

CLINTON S. HOUSH

UNIVERSITY OF MISSOURI-ROLLA

MECHANICAL ENGINEERING & AEROSPACE ENGINEERING

& ENGINEERING MECHANICS DEPARTMENT

ROLLA, MO 65401

GRANT NAG-1-975

MAY 1990

TABLE OF CONTENTS

NOMENCLATURE

b	wing span
$\bar{c}$	Average chord
C_l	rolling moment coefficient
$C_{l_{\delta_a}}$	$\partial C_L / \partial \delta_a$
C_L	lift coefficient
C_{L_α}	$\partial C_L / \partial \alpha$
$C_{L_{\delta_e}}$	$\partial C_L / \partial \delta_e$
C_m	pitching moment coefficient
C_{m_α}	$\partial C_m / \partial \alpha$
$C_{m_{\delta_e}}$	$\partial C_m / \partial \delta_e$
M	Mach number
p	roll rate
q	pitch rate
/R	aspect ratio
S	reference area
α	angle of attack
δ_α	aileron deflection
δ_e	elevator deflection
$\wedge$	sweep angle
Subscripts:	
b	baseline
c.p.	center of pressure
f	front wing
r	rear wing

ABSTRACT

A scissor wing configuration, consisting of two independently sweeping wings has been numerically studied. This configuration has also been compared with an equivalent fixed wing baseline. Aerodynamic and stability and control characteristics of these geometries have been investigated over a wide range of flight Mach numbers.

It is demonstrated that in the purely subsonic flight regime, the scissor wing can achieve higher aerodynamic efficiency as the result of slightly higher aspect ratio. In the transonic regime, the lift to drag ratio of the scissor wing is shown to be higher than that of the baseline, for higher values of the lift coefficient. This tends to make the scissor wing more efficient during transonic cruise at high altitudes as well as during air combat at all altitudes. In supersonic flight, where the wings are maintained at maximum sweep angle, the scissor wing is shown to have a decided advantage in terms of reduced wave drag.

From the view point of stability and control, the scissor wing is shown to have distinct advantages. It is shown that this geometry can maintain a constant static margin in supersonic as well as subsonic flight, by proper sweep scheduling. Furthermore, it is demonstrated that addition of wing mounted elevons can greatly enhance control authority in pitch and roll.

I. INTRODUCTION

The variation of geometry of the aircraft in flight is a relatively old idea. Initially attempts were made to reduce the wing area after take off in order to reduce the total viscous drag of the aircraft. A comprehensive discussion of these attempts is given in Anals of Polymorph (1). With the advent of supersonic flight, the contradictory requirements for slow/fast flight became more pronounced. On the one hand it is desired to have both large aspect ratios and wing areas to minimize the flight speed during landing and take off. On the other hand, at high speeds, especially at supersonic speeds where viscous drag and wave drag dominate the performance, it is attractive to use small lifting surfaces and reduce the frontal area of the aircraft. Also, for low altitude high speed flight it is desired to have small aspect ratios in order to minimize gust loading.

What appeared to be the solution to these contradictory requirements was first proposed in the form of variable sweep. The variable sweep concept was tested extensively at NASA using the X-5 as the test bed (2). It was demonstrated that in order to maintain the aircraft center of pressure within an acceptable envelope the wing root had to be translated forward with increasing sweep. This lead to structural complications. Polhamus proposed a solution (3) which pivots the wings about an outboard location rather than about the center line. At the same time it was proposed that part of the wing should retract into the fuselage with increasing sweep. This outboard pivoting of the wing

provides an acceptable center of pressure shift but further increases the structural weight of the wing due to the outboard nature of the wing pivot. This concept has been widely employed in the F-111, the F-14, the B-1, etc. However, the shifting of the center of pressure at supersonic speeds still remains. It can be argued that this problem can be minimized by fuel transfer and therefore control of the aircraft center of gravity such as that employed in B-1. However, fuel management of this form would be impractical for a fighter/attack configuration due to the instantaneous changes in flight speed that may be required for their missions. Furthermore, these aircraft are of very compact design, leaving very little room inside for large fuel transfers required to control the center of gravity.

The idea of the oblique wing, introduced by R. T. Jones (4), is another attempt at alleviating the problems of the conventional variable sweep. Although the apparent simplicity of this concept is very attractive, at large sweep angles the coupling between the longitudinal and the lateral modes of the aircraft lead to unacceptable handling problems. Namely, at large sweep angles the deflection of ailerons induces a pitching moment which is antisymmetric. Furthermore, the leading edge suction at high sweep angles tends to induce a side slip which has to be countered by either tilting the wing or flying with a constant bank angle. The former solution adds to the structural complexity, while the latter is totally unacceptable from the view point of handling quality.

Rokhsaz in (5) and (6) introduced a new variable geometry

design, called the scissor wing. Two wings are used in this concept, both pivoted about their mid span. A typical scissor wing layout is shown in Figure 1 in both the unswept and swept configurations. At low speeds the sweep is minimized in order to reduce the induced drag and increase the maximum lift coefficient and the lift curve slope. At supersonic speeds the two wings are swept in opposite directions. This arrangement allows the designer to either choose a minimum drag configuration or control the static margin over a range of Mach numbers, with each of these choices imposing ideally a small penalty in terms of the other. Also the reduced aspect ratio associated with sweep reduces the aircraft lift curve slope at high speeds, therefore reducing gust loading. Furthermore, this arrangement has none of the handling problems of the oblique wing due to its total symmetry. Additionally, this unique configuration allows the designer to manipulate the static margin and longitudinal control of the aircraft through wing sweep. The center line pivot point allows for lower wing structural weight than the currently used variable sweep designs with the outer span pivot points.

This research intends to demonstrate the advantages of a scissor wing configuration compared with an equivalent fixed wing geometry. Aerodynamic, as well as some stability and control aspects of the scissor wing are to be investigated using a number of numerical models. All computer codes used for this purpose, with the exception of NARUVLE and VPANEL, have been provided by NASA Langley Research Center.

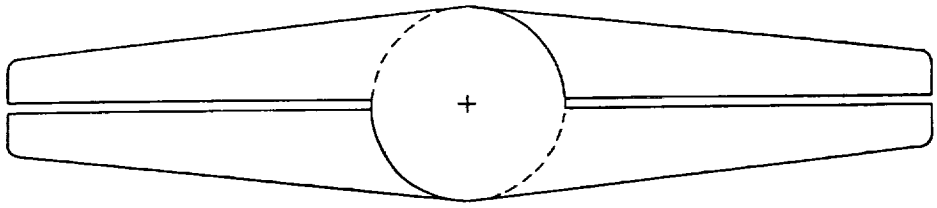

NO SWEEP

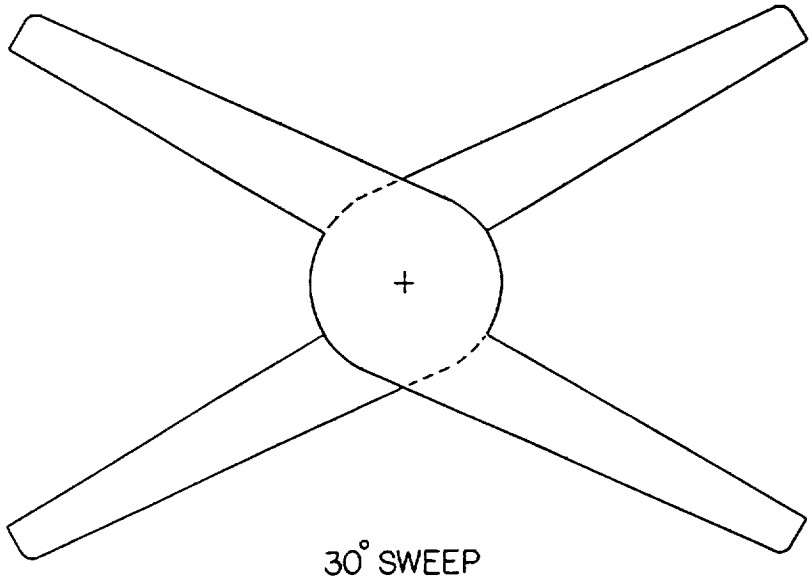

30° SWEEP

Figure 1. Scissor Wing Configuration.

II. MODELING

A. NUMERICAL MODELS

1. Induced/Wave Drag Due to Lift: The linear vortex lattice method of Tulinius (7), NARUVLE, was used to calculate the induced drag and wave drag due to lift as well as the stability and control derivatives. This code uses the Prandtl-Glauert transformation in the subsonic range, and supersonic vortices in the supersonic range. Therefore, this method of analysis was limited to the linear range of aerodynamics. This precluded any high angle of attack calculations as well as the transonic flight regime. VORCAM, a program developed by E. Lan (8), was also initially used for these predictions. However, since the lift and drag results of NARUVLE and VORCAM were in excellent agreement only NARUVLE was used for the detailed studies. NARUVLE was chosen because it was more readily modified to iteratively trim the aircraft for a given set of wing loading, flight Mach number, and dynamic pressure. Furthermore, this code is capable of modeling any arbitrary number of the lifting surfaces. This allowed modeling of all lifting surfaces under trim in one step.

For obtaining the stability and control derivatives of the configurations, all lifting surfaces were represented by symmetric thin surfaces, including the strake. The program was not able to account for the effects of the fuselage and was also limited to two hundred panels. This resulted in slight numerical

oscillations in a few cases. Although the absolute results predicted by this model may not be quantitatively accurate, the predicted trends are valid. Also, firm conclusions can be drawn when this method is used for comparison of two geometries. Within the above constraints NARUVLE was capable of modeling both wings, the center surface, and the horizontal stabilizer.

Since NARUVLE could predict only the induced drag and wave drag due to lift under trim, a component drag build up method was used to estimate the total configuration drag. The viscous drag of the configurations was separated into two parts. The first part was assumed to be due to the fuselage. Using methods of Nicolai (9) the value of this drag coefficient was calculated and was assumed to depend on the Reynolds number only. For lifting surfaces, the airfoil specified by NASA was the 6 percent thick NACA 64A-006. Since most calculations were performed at high speeds where the lift coefficient was small, the viscous drag coefficient of all lifting surfaces was assumed to remain constant and inside the drag bucket of this airfoil. In supersonic cases, the zero lift wave drag of the configurations was estimated using a separate code and added to the other components.

2. Zero Lift Wave Drag: The zero lift wave drag of the configuration was calculated using the program WDRAG2 (10). This program employs Whitcomb's method of area ruling. Twelve azimuthal cutting planes along with seventy longitudinal stations were used assuring converged results in all cases. Figure 2 shows the convergence history of WDRAG2 for different number of longitudinal cutting planes.

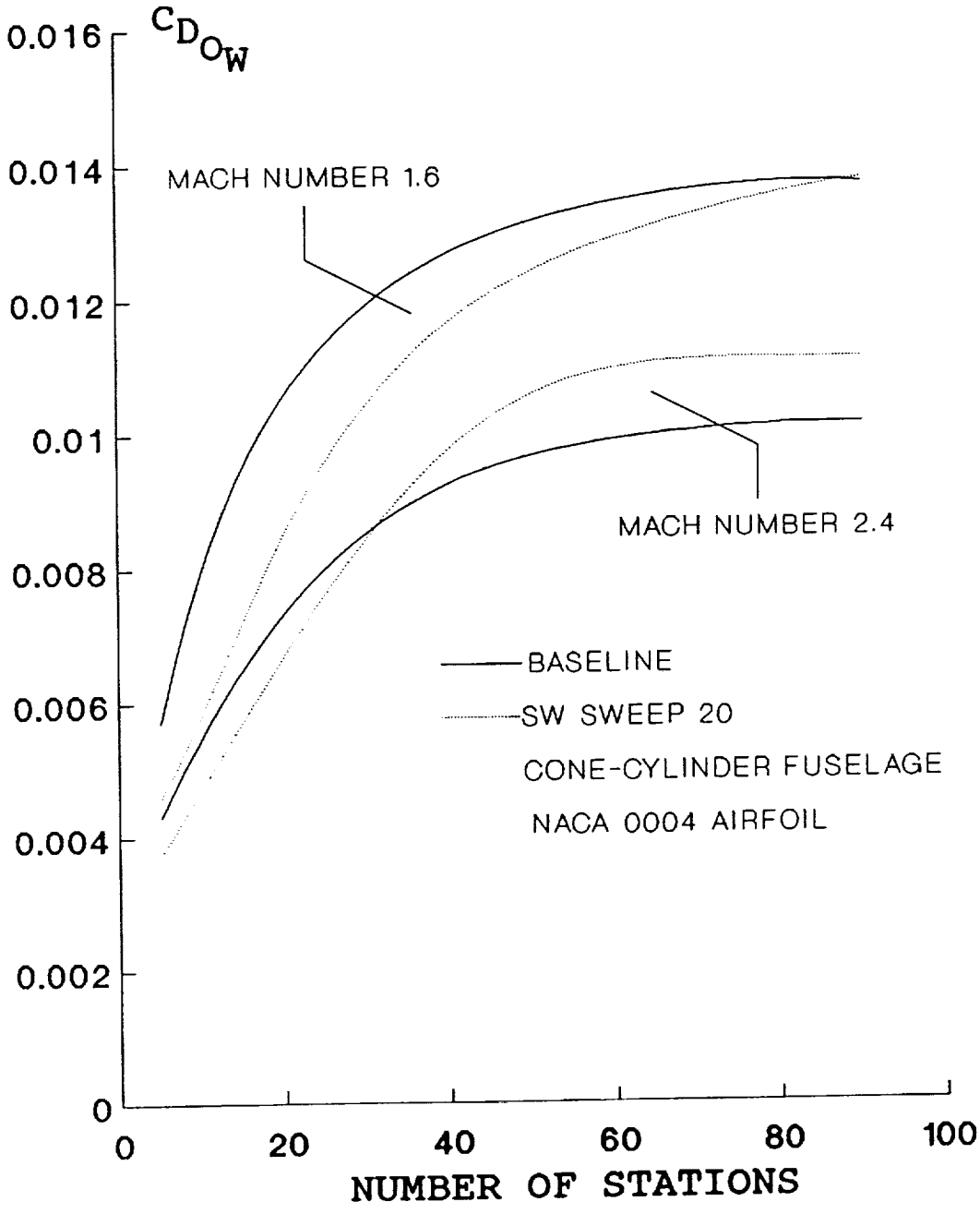

Figure 2. Convergence History of WDRAG2.

Two vertical surfaces were canted three degrees from the horizontal to model the horizontal stabilizers. The rear wing and the circular center section were modeled as one surface, and the front wing as a second horizontal surface. The fuselage was modeled in most cases as a axisymmetric cone cylinder body.

3. Transonic Flow: Transonic flow calculations were made with CANTATA which is an extension of that due to Boppe, (11). This code uses a finite difference method to solve the three dimensional transonic small perturbation equations. Viscous effects are estimated here using momentum integral techniques. This code can allow for a floating wake and vector processing, and was developed by P. Aidala (12). CANTATA could only handle two lifting surfaces, i.e., a wing and tail or a two piece wing. Thus all CANTATA cases were run without a horizontal stabilizer, and therefore were un-trimmed. CANTATA was utilized to assess whether any unusual transonic problems materialized for the scissor configuration. Some work was done with wings and a fuselage, however, most of the analysis was with just the wings. Also, CANTATA would not run with two wings with zero or small gap. Therefore, all CANTATA calculations were performed with a gap of approximately 25% of the chord.

4. Two Dimensional Aerodynamic Coupling: A two dimensional vortex panel code, VPANEL, was used to analyze the detail coupling effects between the airfoils. This code was developed at University of Missouri-Rolla. VPANEL uses the vortex panel method of Stevens et al (13) along with a number of momentum integral techniques to estimate the two dimensional viscous drag.

This code was primarily used to asses the best decalage angle between the wings from the view point of viscous drag. This code also demonstrated that these decalage effects can be simulated using leading edge flaps.

B. AIRPLANE MODELS

For the purpose of comparison, two configurations were considered; a fixed wing aircraft, and an equivalent scissor wing geometry. Both configurations had a common fuselage, common stabilizer surfaces, and equal total wetted area. These aircraft were assumed to represent a typical attack aircraft at maximum gross take off weight. The stabilizer was assumed to act as the elevon in all cases, with 12% chord ratio ailerons on the wings. The horizontal stabilizer of the scissor wing was placed at 8.5% of the span below the wing to avoid geometric interference between the two. For the baseline, the stabilizer and the wing were in the same plane.

1. Baseline: The weight of the baseline was set at 50,000 pounds with a wing loading of 117.3 pounds per square foot. The baseline had a trapezoidal wing with aspect ratio of 4.18 and leading edge sweep angle of 23 degrees.

2. Scissor Wing: The weight of the scissor wing was also set at 50,000 pounds. Having the same wing area as the baseline resulted in the same wing loading of 117.3 pounds per square foot. The scissor wing at zero sweep had an aspect ratio of 4.27 compared with 3.63 for the baseline. The scissor wing at a sweep

angle of 17 degrees had the same aspect ratio as the baseline. The baseline and the scissor configuration at four different sweep angles are shown in Figure 3.

3. Canarad Configuration: For the above scissor wing a canard configuration was also devised with the same canard area as the horizontal tail area. The wing loading and the total weight were the same as that of the above cases. The static margin in these cases was changed by moving the canard relative to the wing. A 5% stable case and a 9% unstable case were used for the purpose of comparison.

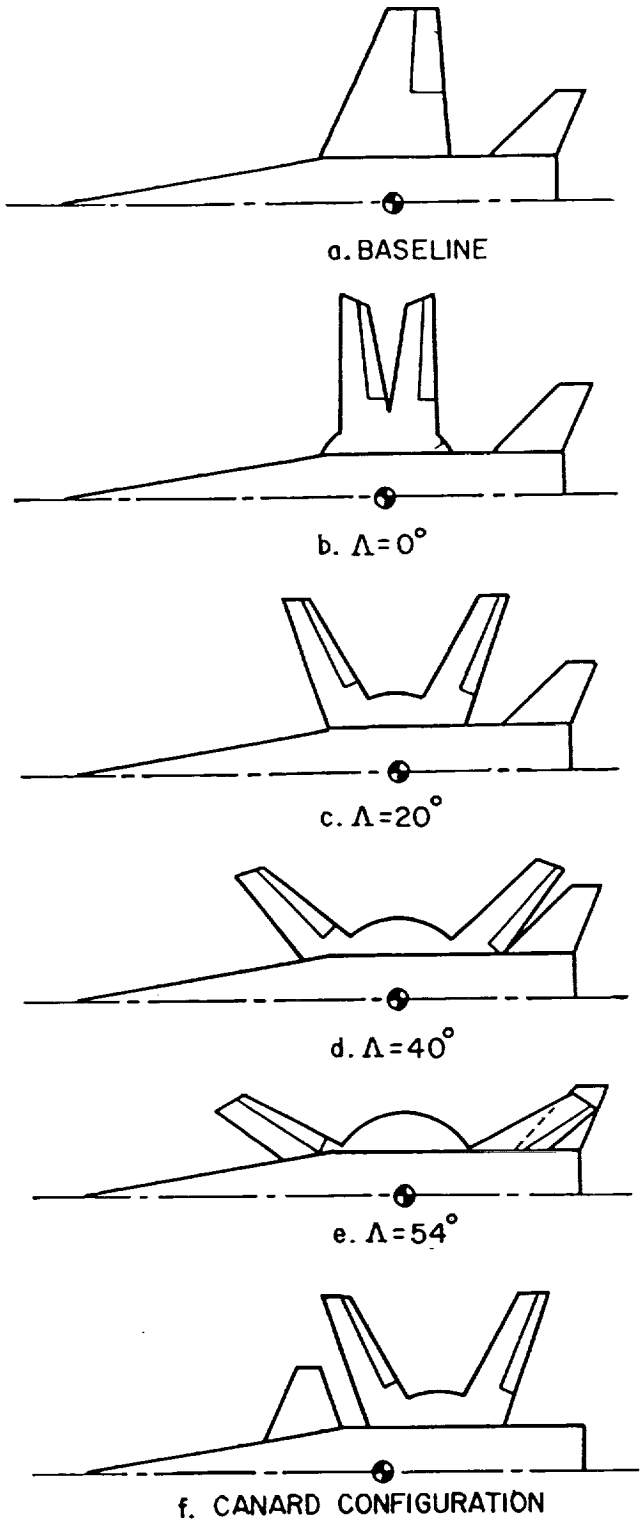

Figure 3. Baseline and Scissor Wing Configuration.

III. ANALYSIS

A. SUBSONIC FLIGHT

Subsonic aerodynamics and stability and control of the configurations were analyzed using NARUVLE. All configurations were trimmed and all drag data was obtained from the component drag build up.

1. Aerodynamics: For these initial studies, the scissor wing of Figure 1 was used to establish trends about the shifts in the center of pressure. Figure 4 shows the lift curve slope of this geometry. As expected, lift curve slope decreases with increasing sweep angle. This is not only due to the increased sweep, but also due to reduced effective aspect ratio. In this figure, Mach numbers of 0.75 to 1.25 were omitted because they were clearly in the transonic range and out of the domain of validity of the computer program. Figure 5 shows the center of pressure for the same geometry at different values of the sweep angle and Mach number. It is clearly evident from this figure that the center of pressure of the wing shifts forward with increasing sweep angle. This is the direct consequence of the aerodynamic coupling between the wings. In the presence of such coupling, the lift curve slope of the front wing is much larger than that of the uncoupled wing, while the lift curve slope of the rear wing is much smaller than that of a single wing. Therefore, increasing the sweep angle causes the overall center of

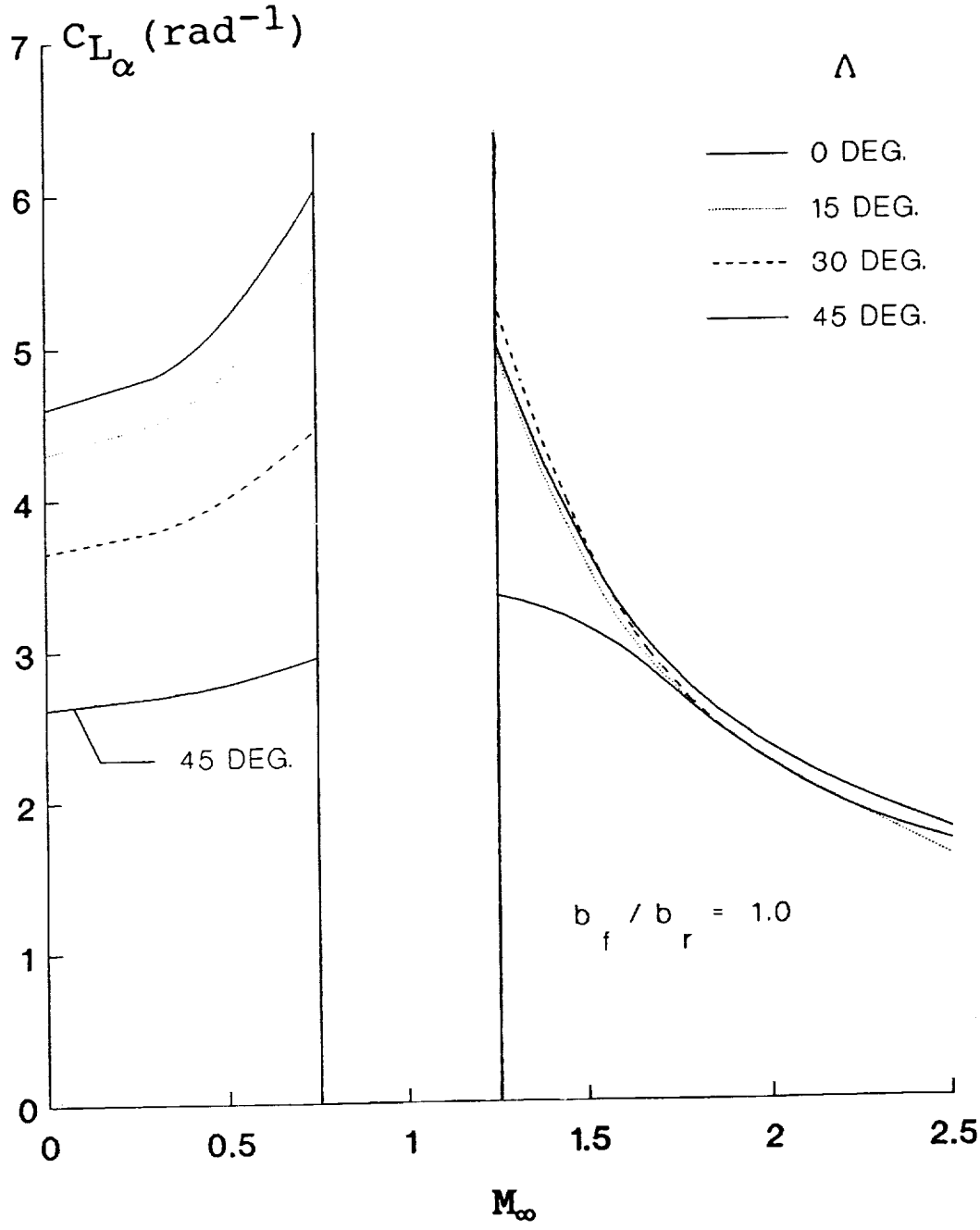

Figure 4. Lift Curve Slope for Equal Spans.

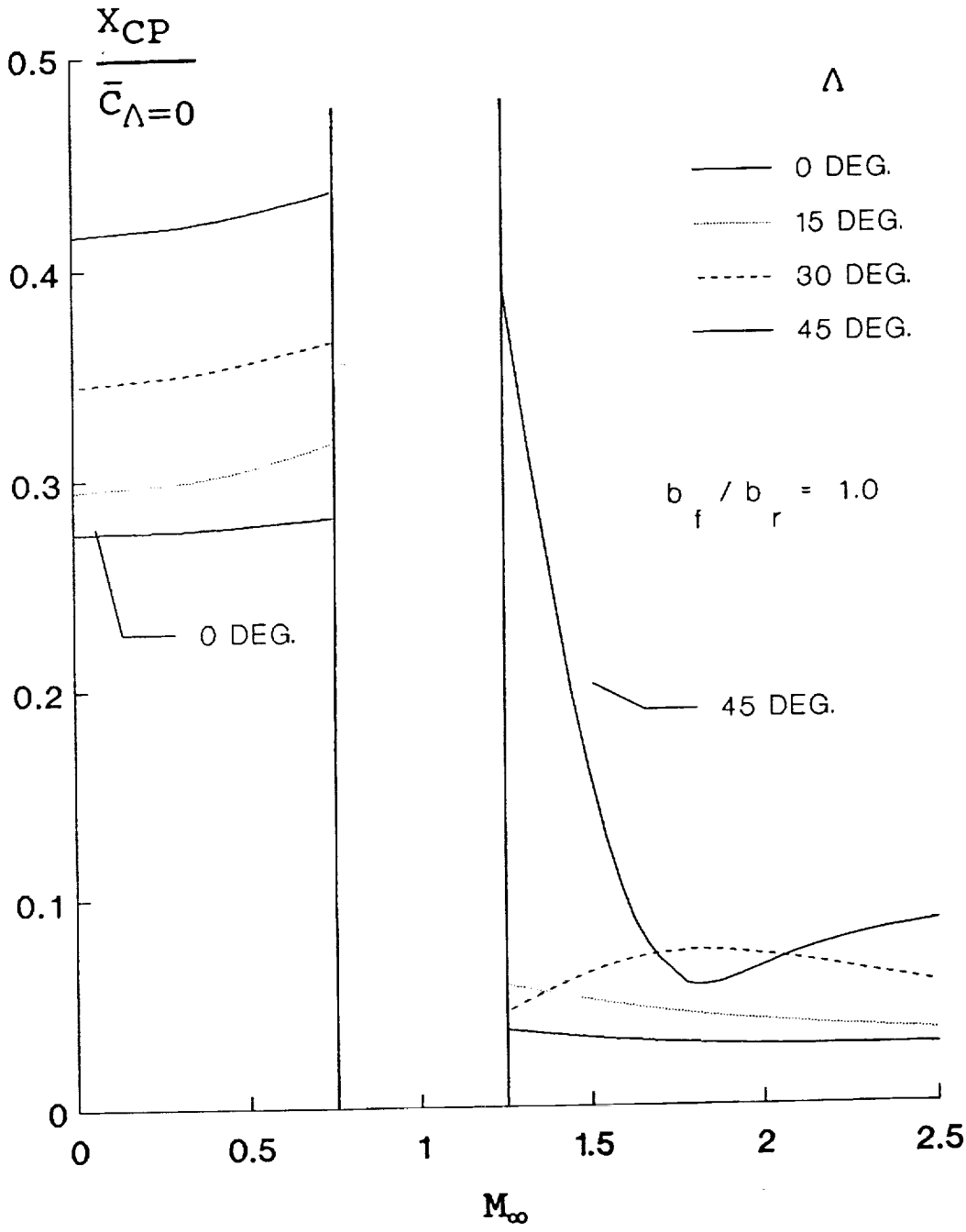

Figure 5. Center of Pressure Relative to the Pivot for Equal Spans.

pressure to move slightly forward. As the sweep angle increases this coupling tends to diminish. Since this point and the aerodynamic center of the wing are closely associated, this behavior would indicate a decrease in the static margin of an aircraft if it were to be equipped with this wing.

In order to demonstrate that these shifts of the center of pressure can be manipulated to an optimum degree by the aircraft designer, this parameter was calculated for another geometry as well. Figure 6 represents the results for a wing similar to that of Figure 5, except with the front wing having twice the chord length of the rear wing. Figure 6 shows that variation of the sweep angle would cause large changes in the center of pressure. However, in this case, there is very little difference in the location of this point between a sweep of 15 degrees in subsonic flow and 45 degrees in supersonic flow. Therefore, it remains to the designer to choose the proper chord and span ratios in order to accommodate the specific design requirements.

Using NARUVLE and the geometries depicted in Figure 3 aerodynamic studies were conducted of the scissor and baseline configurations. Figure 7 shows the ratio of the lift coefficient to the sum of the induced drag and wave drag coefficients due to lift and viscous drag. These results were obtained under trim for all configurations at sea level. The transonic range in this figure is an interpolation between the subsonic and supersonic ranges. This was required because NARUVLE had no transonic capability. At low subsonic Mach numbers the lift to drag ratio of the scissor is slightly superior to the baseline. At Mach numbers

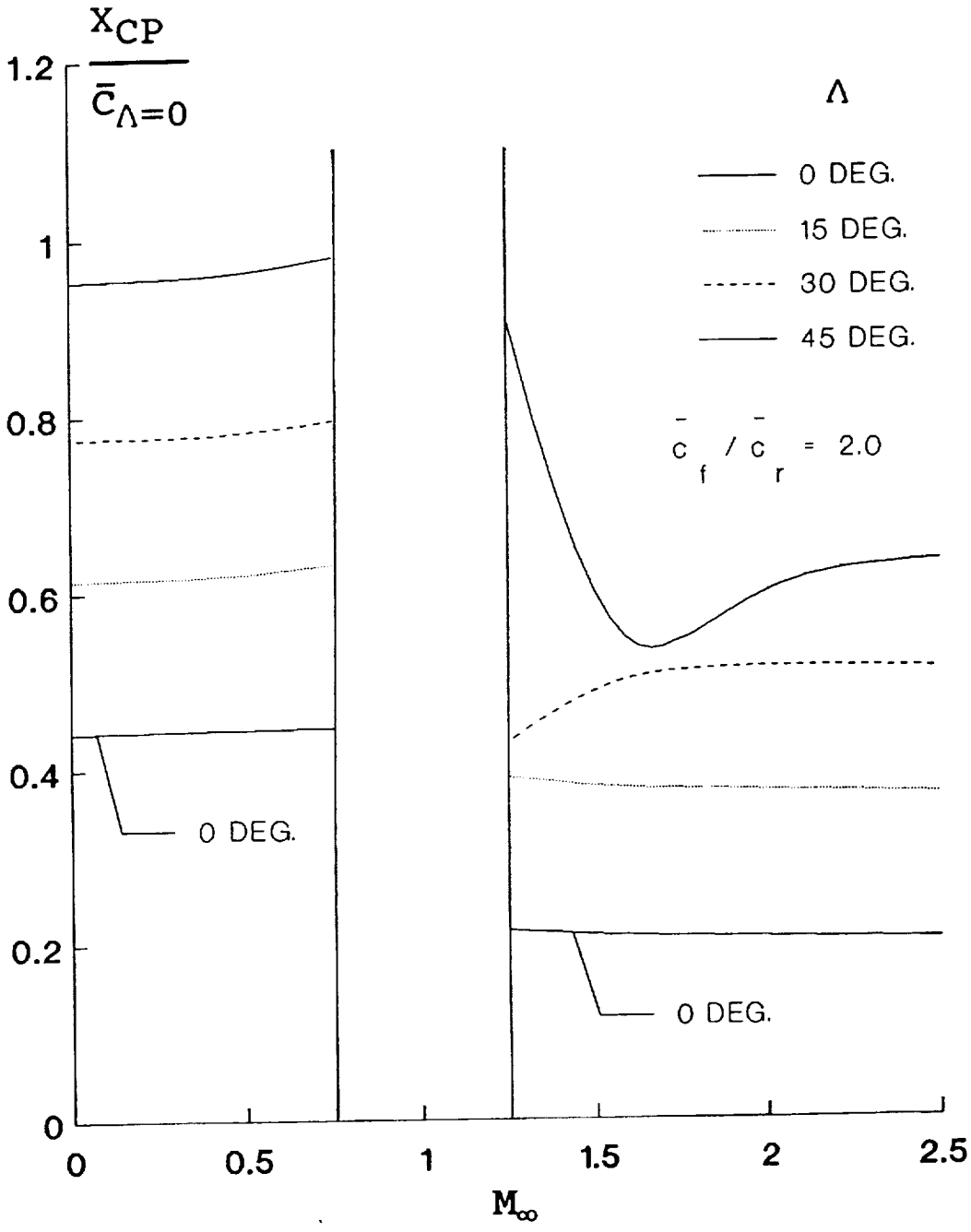

Figure 6. Center of Pressure for Unequal Chords.

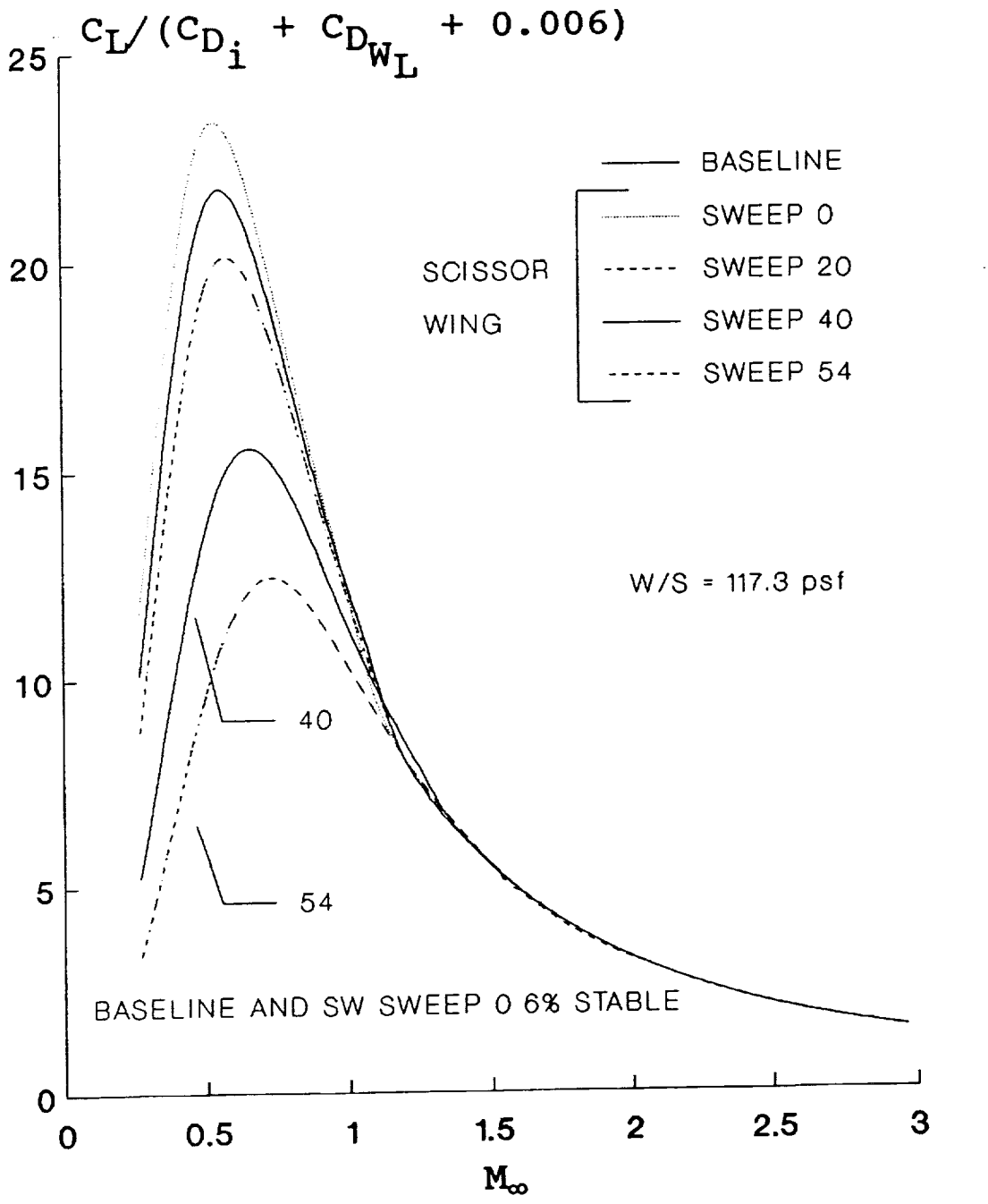

Figure 7. Lift to Drag Ratio from NARUVLE for Equal Aspect Ratios.

above 1.25 the baseline is slightly superior to scissor except when the scissor is at zero sweep. Aspect ratio effects were studied by varying both wings' spans and chords while keeping the total area constant. Figure 8 shows the effect of varying aspect ratio with span changes. As the aspect ratio of the forward wing to rear wing increases from 1.0 to 1.44, for sweep angles of 0 and 20 degrees, the lift to drag ratio increases in Mach number range from 0.4 to 0.8. Supersonically there is no change. As sweep angle increases the increased lift over drag from aspect ratio is diminished. Figure 9 shows the effect of varying the aspect ratio by changing the chord ratio. The results shown here indicate an insignificant effect on the lift to drag ratio over the entire Mach number range. Similar trends would be expected for both span and chord variations if the aspect ratio of the front to the aspect ratio of the rear wing were less than one by the inverse of 1.44 as discussed above.

Canard scissor configurations were also studied with NARUVLE. The 5 percent stable static margin case is shown in Figure 10 for both 0 and 20 degree sweep angles. In both cases the canard has less lift to drag ratios than the conventional scissor-tail, with the 0 sweep case being the most pronounced. Figure 11 illustrates the 9 percent unstable static margin case for the canard-scissor configuration. In this instance the canard configuration is slightly improved over conventional scissor especially at the 0 degree sweep. But again this occurs only in a very narrow Mach number region.

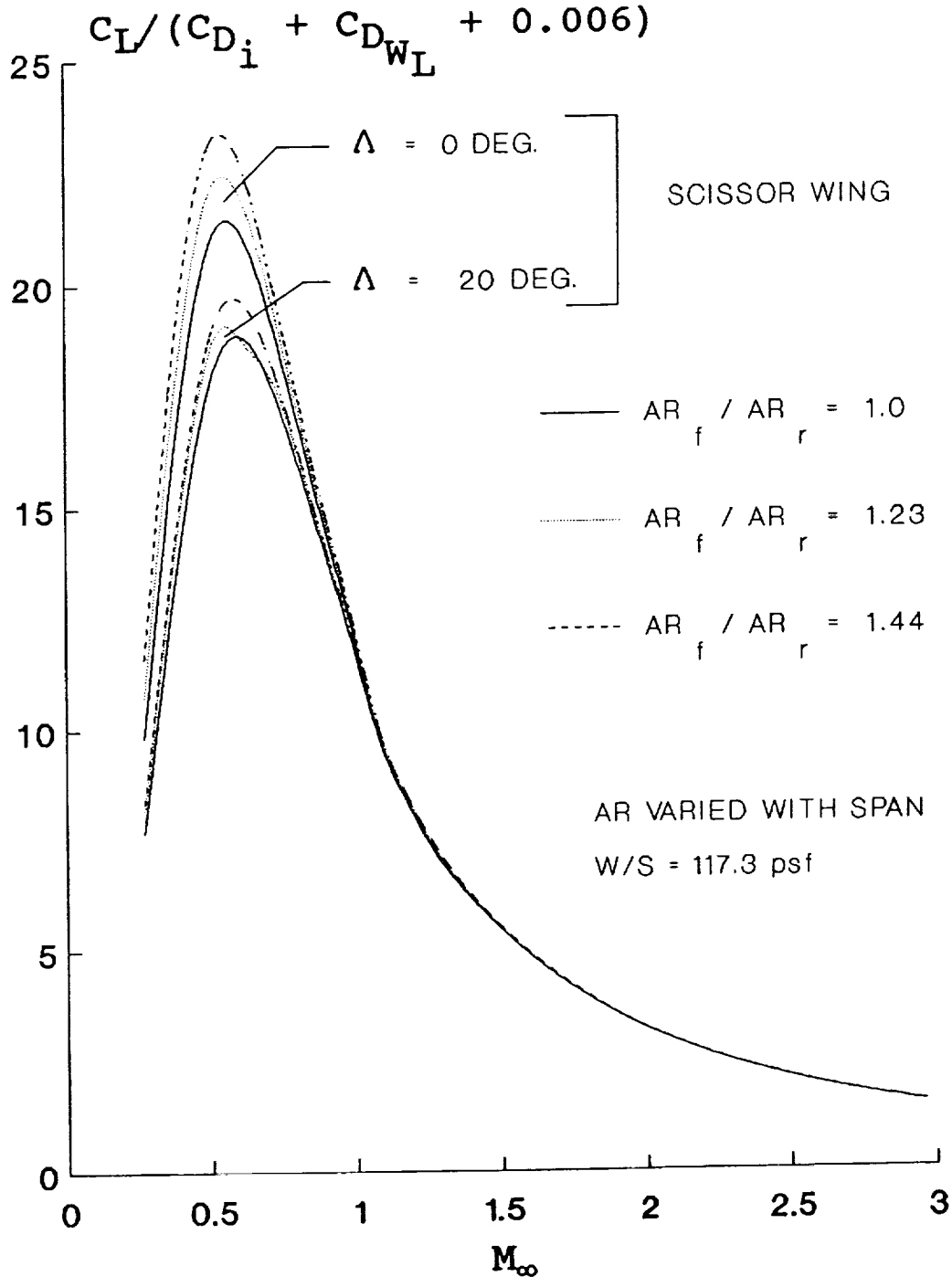

Figure 8. Effect of Span Variation on Lift to Drag Ratio .

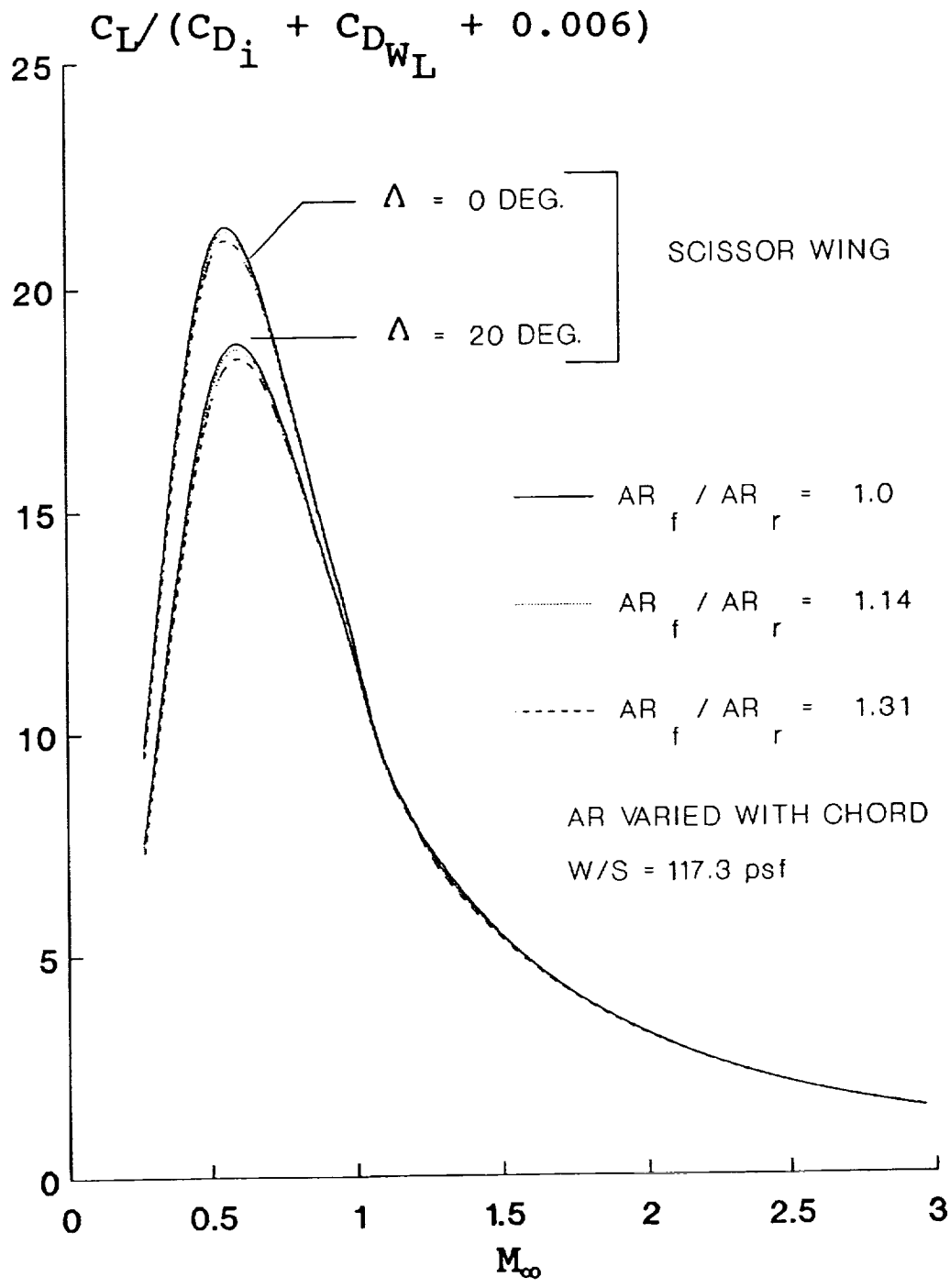

Figure 9. Effect of Chord Variation on Lift to Drag Ratio.

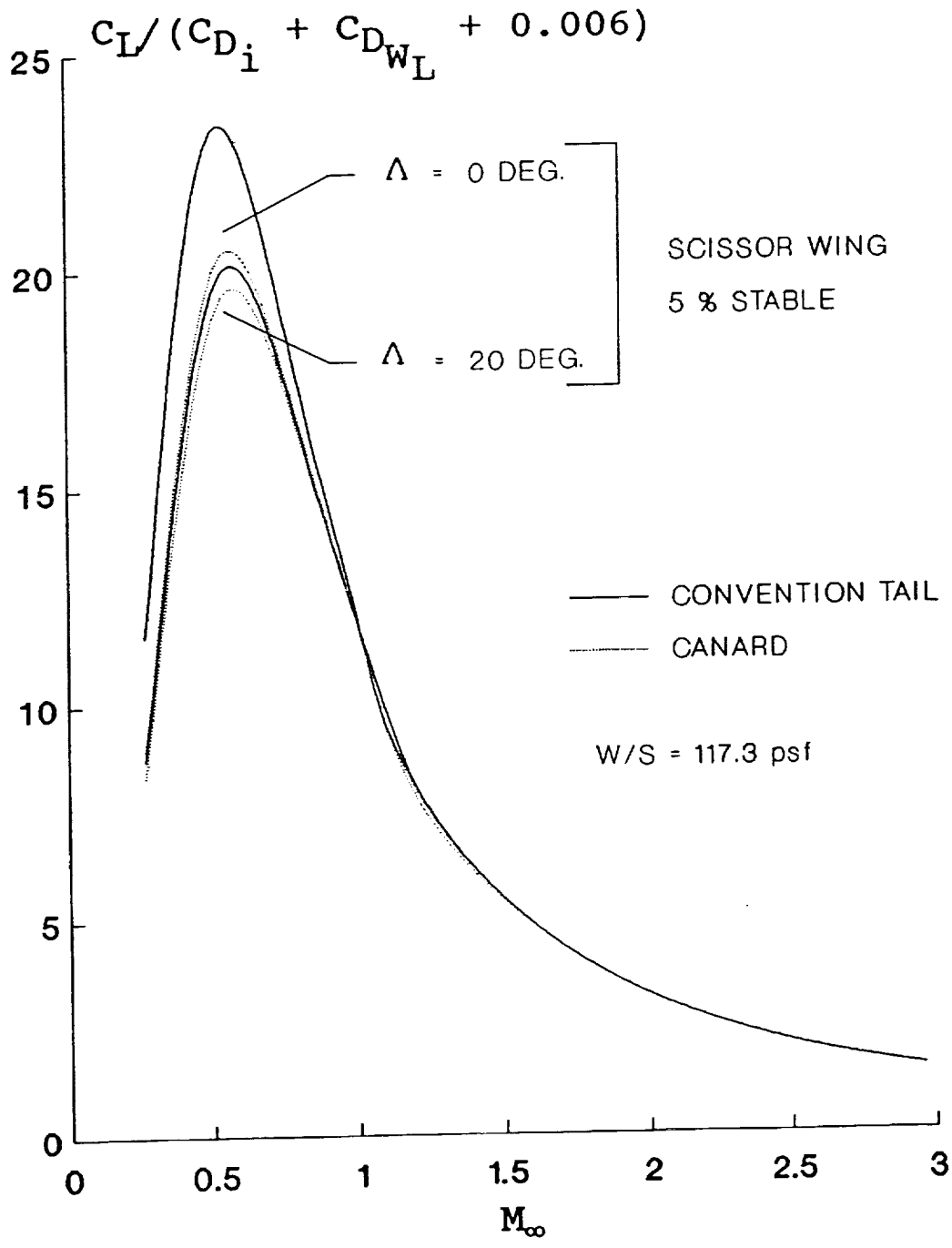

Figure 10. Comparison of Conventional and Canard Scissor Wings, 5% Stable.

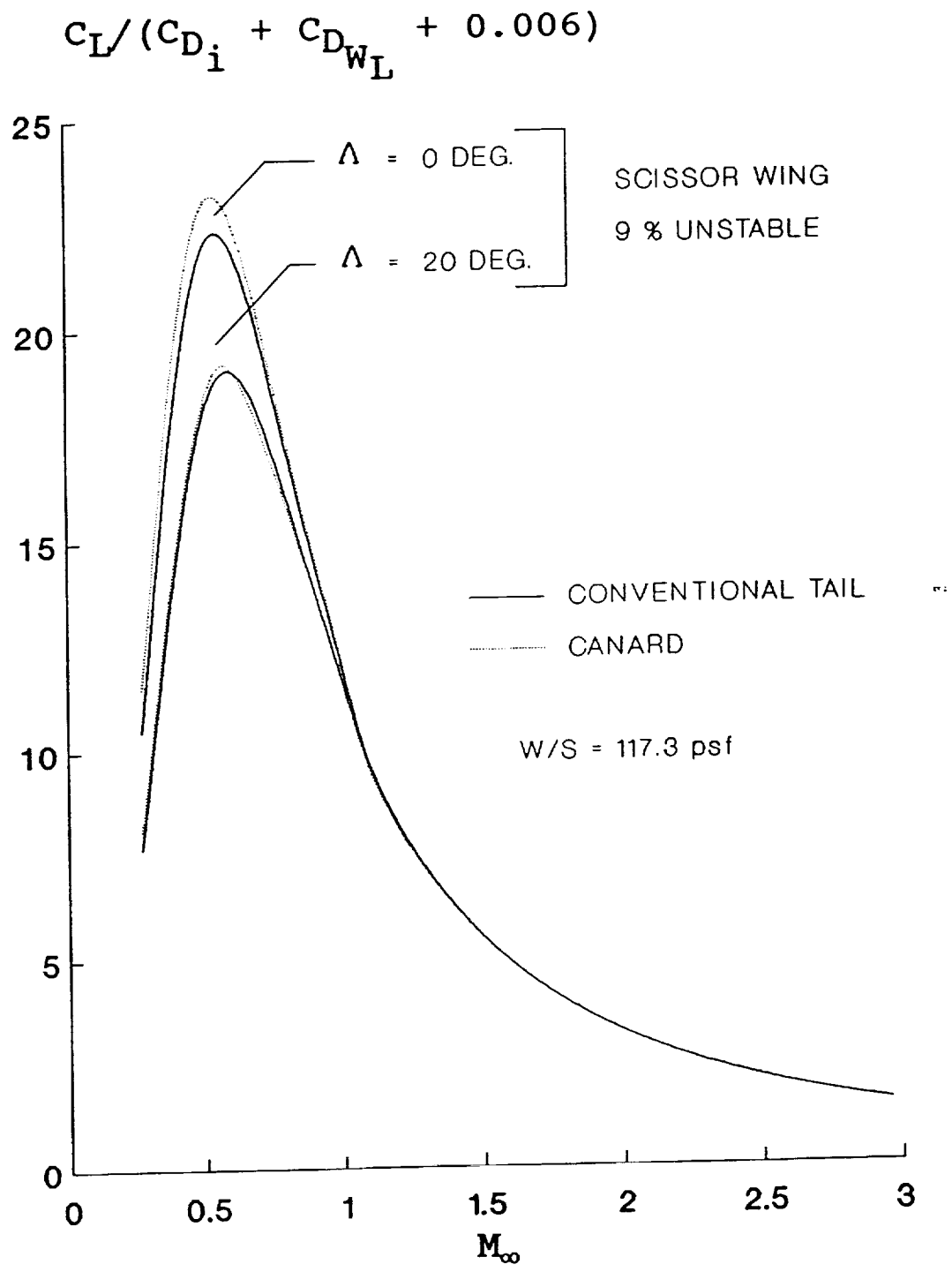

Figure 11. Comparison of Conventional and Canard Scissor Wings, 9% Unstable.

From the view point of viscous drag, in the presence of strong aerodynamic coupling, a samll amount of negative decalage is always needed at subsonic speeds. On the other hand, at supersonic speeds, this decalage can become a detriment. The solution to these conflicting requirements is to use no decalage and instead simulate this effect by deploying leading edge and trailing edge flaps on the front and the rear wings, respectively. Figures 12 and 13 show the potential of this scheme as predicted by VPANEL. These figures show clearly that; 1) the decalage effects can be simulated by these flaps, and 2) the drag bucket can be shifted to any desired lift coefficient.

2. Stability and Control: Geometries represented in Figure 3 were used to study the effectiveness of different control surfaces. All these derivatives were calculated at zero Mach number for varying sweep angles. However, the effects of Mach number on the longitudinal static stability of the aircraft was also considered. All moments were taken about a fixed assumed center of gravity location resulting in -15% static margin at zero Mach number for the baseline and zero sweep for the scissor wing. The pivot was assumed to be at the mid chord of the wing root and the wings had equal spans. In the swept cases, even though the exposed area, the wing span, and the effective chord were different, those of the unswept configuration were used as reference quantities. The effectiveness of every control surface was calculated at zero angle of attack by dividing the respective forces and moments by the small corresponding control surface deflection. These results are presented in the following sub-

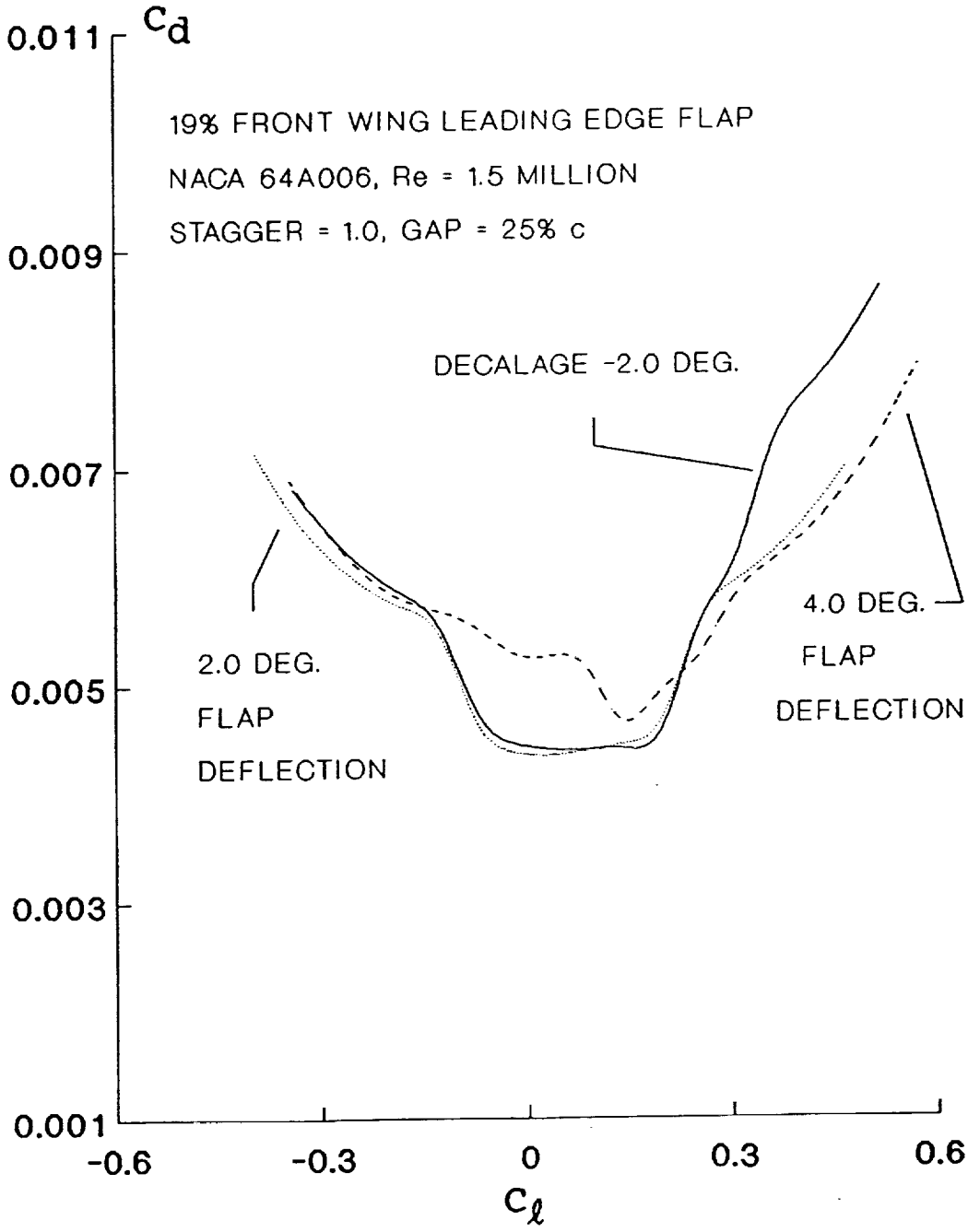

Figure 12. Effect of Leading Edge Flap on Viscous Drag.

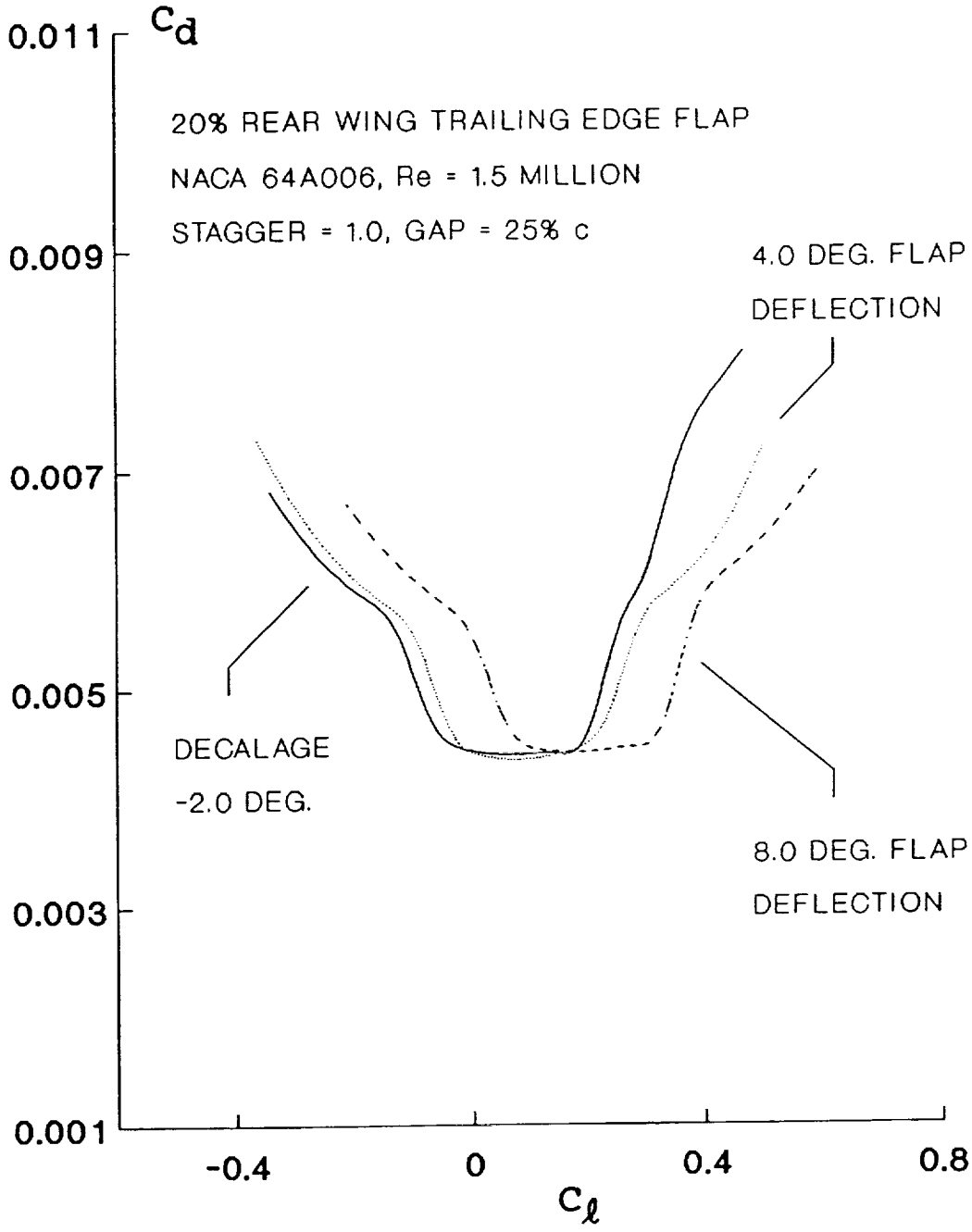

Figure 13. Effect of Trailing Edge Flap on Viscous Drag.

sections.

i. Longitudinal Control: Figure 14 shows the effects of the elevator deflection on the total aircraft pitching moment coefficient. Since the horizontal tail locations were not the same, these derivatives are slightly different for the scissor wing and the baseline. As expected, the effectiveness of the wing mounted elevons somewhat diminishes with increasing sweep angle. However, this does not necessarily translate into loss of elevator authority. As the sweep angle increases, the effective lifting area of the aircraft decreases. Furthermore, as it is evident in Figure 14, the front wing elevons now begin to offer a strong influence on the aircraft pitching moment. This is quite natural because at moderate sweep angles, the scissor wing configuration becomes very similar to a three surface geometry. In fact under these conditions, the combination of the tail and front wing can be used to trim the aircraft at arbitrary attitudes for a fixed airspeed. If a scissor at 40 degrees of sweep were at M=0.8 it could be trimmed over a range of angle of attack of 5.5 degrees angle of attack.

Figure 15 shows the pitch damping derivative as function of the sweep angle at zero Mach number. As would be expected this derivative sharply rises with increasing sweep. However, this should not result in any significant loss of control authority. To demonstrate this point, one can consider the following approximation. About the pitch axis

$$(i_B D - C_{m_q})\hat{q} = C_{m_{\delta_e}} \delta_e \qquad (1)$$

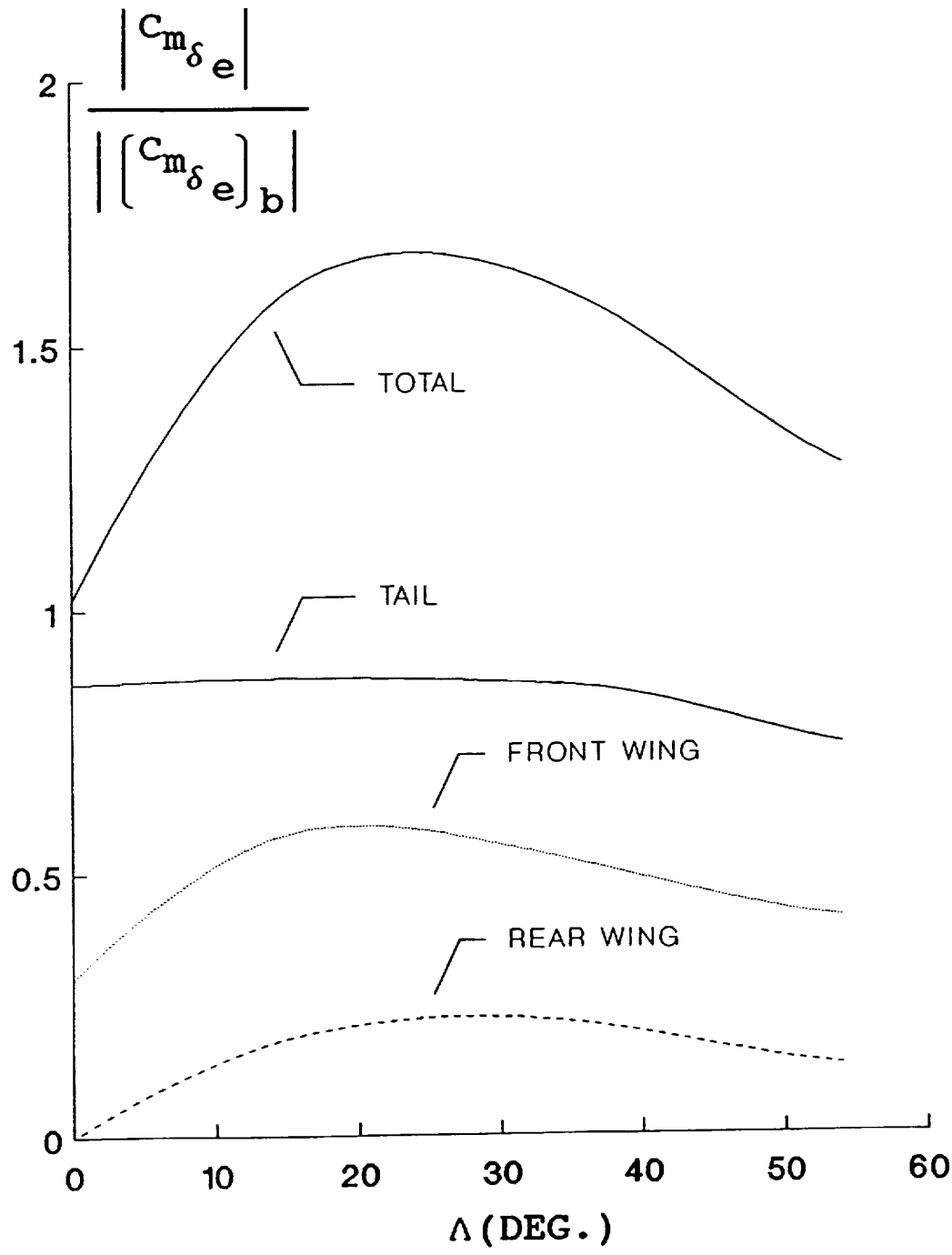

Figure 14. Pitch Control Derivative at $M_\infty = 0$.

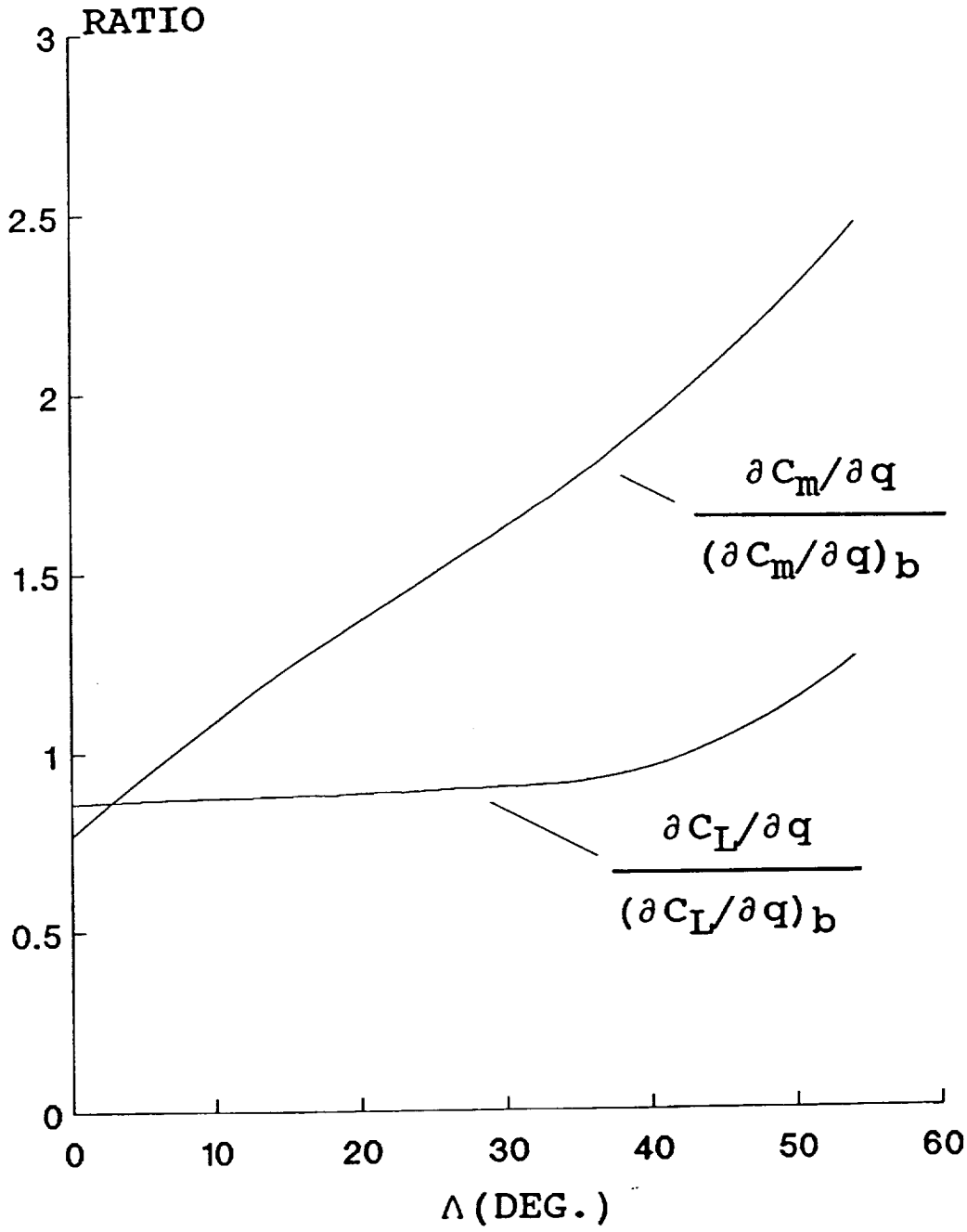

Figure 15. Pitch Damping Derivative at $M_\infty = 0$.

where $\hat{q}$, $\hat{t}$, and i_B represent the non-dimensional pitch rate, time, and mass moment of inertia, respectively. In response to a unit step function deflection of the elevator,

$$\hat{q} = C_{m_{\delta_e}} \delta_e [\exp(\frac{C_{m_q}}{i_B} \hat{t}) - 1]/C_{m_q} \tag{2}$$

$$\hat{Dq} = C_{m_{\delta_e}} \delta_e \exp(\frac{C_{m_q}}{i_B} \hat{t})/i_B \tag{3}$$

Now if control authority is defined as the initial angular acceleration of the aircraft due to the elevator input (i.e. t = 0), then

$$\frac{\hat{Dq}(\hat{t} = 0)}{\delta e} = \frac{C_{m_{\delta_e}}}{i_B} \tag{4}$$

As the sweep angle increases, the mass moment of inertia about the pitch axis also increases. However, since $C_{m_{\delta_e}}$ is much larger than that of the baseline, increasing i_B will not affect the pitch authority compared with the baseline. On the other hand, if control authority is defined as the ultimate pitch rate (i.e. $\hat{t} \to \infty$), then

$$\frac{\hat{q}(t \to \infty)}{\delta e} = \frac{C_{m_{\delta_e}}}{C_{m_q}} \tag{5}$$

In this case, as the sweep increases, C_{m_q} increases resulting in some loss of pitch rate. However, this loss will not be realized until sweep angle becomes larger than approximately 40 degrees, as indicated from Figures 14 and 15.

ii. Lateral Control: Figure 16 shows the aileron effectiveness of the geometry under consideration. It is quite evident from this figure that the effectiveness of the wing mounted ailerons diminishes quite rapidly with sweep. But the tail appears to remain insensitive to the wing sweep, despite the strong aerodynamic coupling between the two. Again, much like the longitudinal case, the apparent reduction in the aileron effectiveness should not be any cause for alarm for the following reasons:

1. This derivative is a function of the wing area and the wing span. Both of these parameters decrease with increasing sweep. However, these effects are not reflected in Figure 16 because the reference area and span were maintained constant throughout these calculations.
2. Roll damping derivative also decreases rapidly with sweep, as shown in Figure 17.
3. The mass moment of inertia of the aircraft about the roll axis decreases with the square of the cosine of the sweep angle.

A simple model similar to that of the previous sub-section will demonstrate that control authority in this mode actually increases with increasing sweep angle.

iii. Longitudinal Stability: Lift and pitching moment curve slopes are depicted in Figure 18. As shown here, lift curve slope decreases predictably with increased sweep angle. Reference was made to reduced gust loading at large sweep angles. This parameter is directly proportional to the aircraft lift

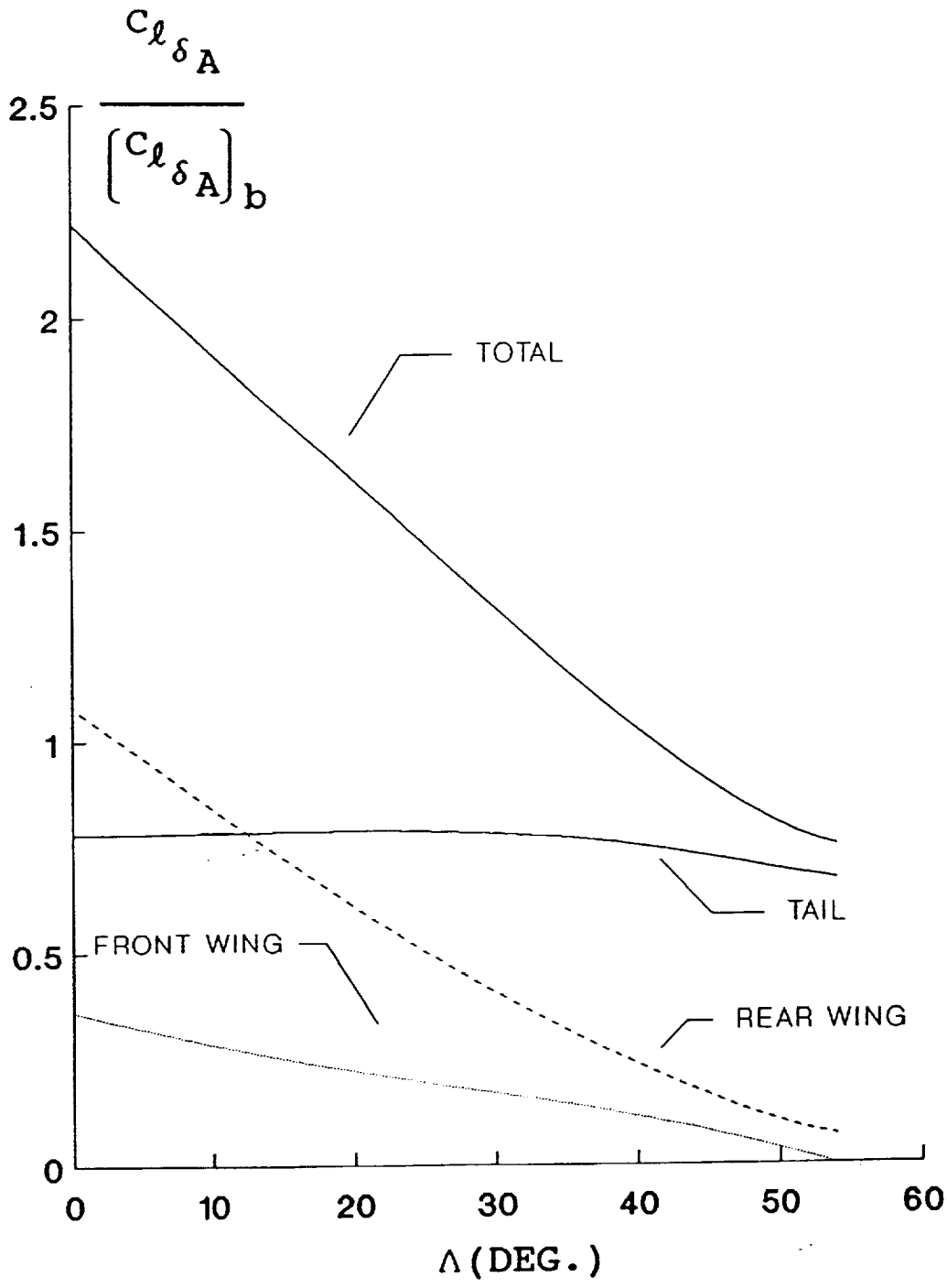

Figure 16. Roll Control Derivative at $M_\infty = 0$.

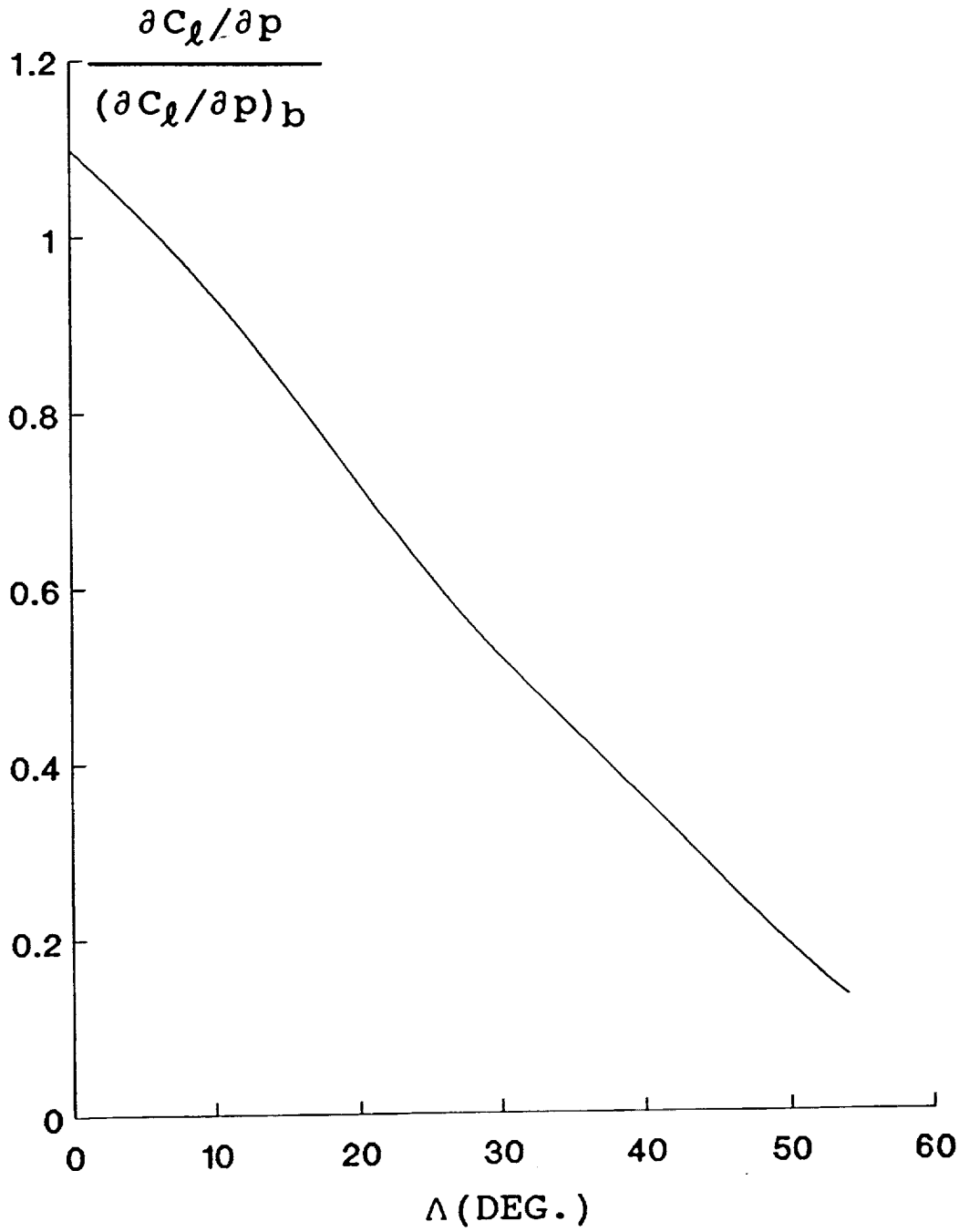

Figure 17. Roll Damping Derivative at $M_\infty = 0$.

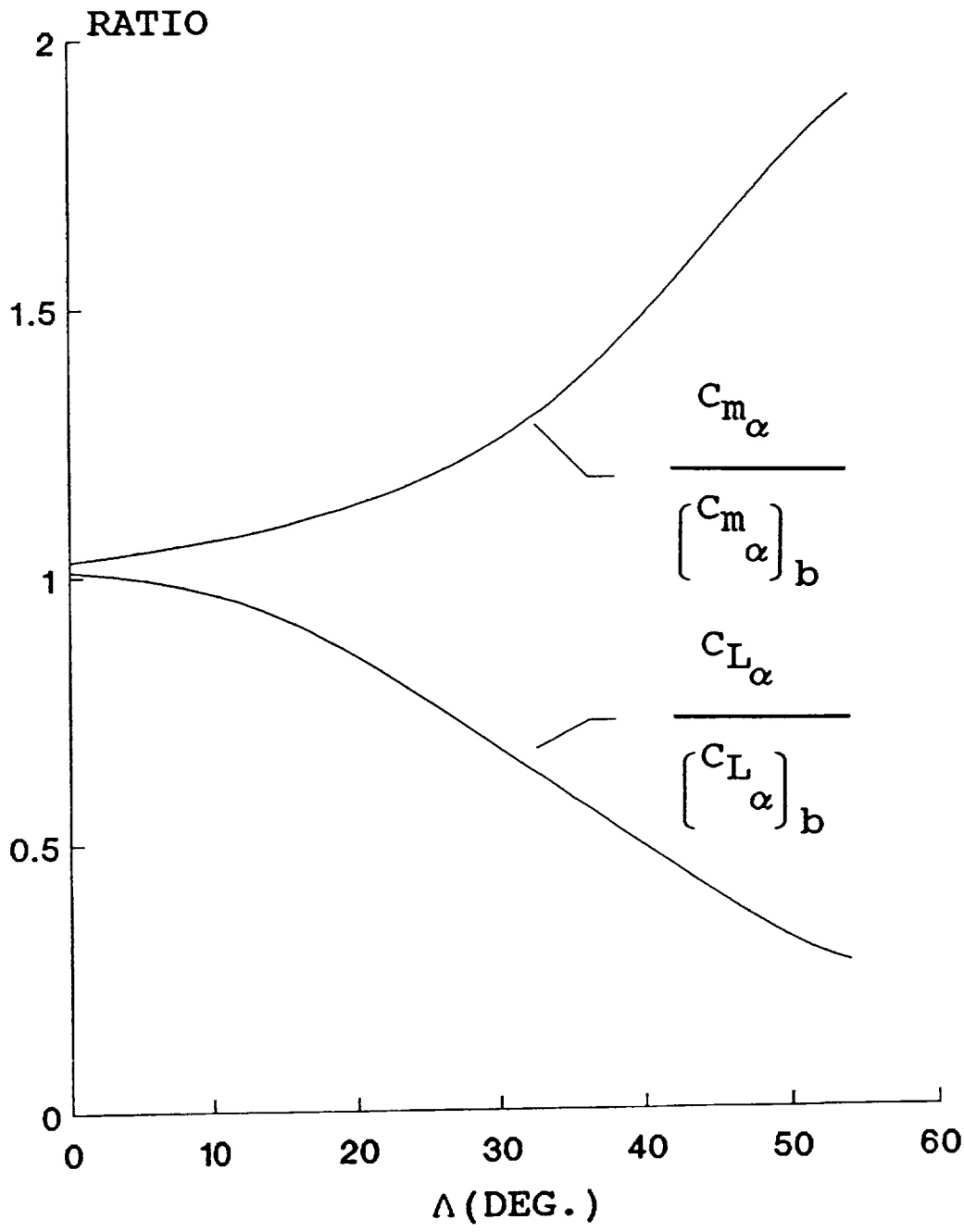

Figure 18. Lift and Pitching Moment Slopes at $M_\infty = 0$.

curve slope. Therefore, any reduction in this derivative results in reduced gust loading with all other parameters being the same. The reader should be cautioned that although the magnitude of C_{m_α} increases with increasing sweep angle, this actually indicates a reduction in longitudinal stability. The reason for this rests in the fact that all configurations considered here were statically unstable. This can be more clearly seen in Figure 19. Static margin in these figures was calculated from the ratio of ΔC_{m_α} and ΔC_{L_α}. This figure clearly indicates a reduction in longitudinal stability as function of sweep angle which is consistent with the results shown in Figure 5. Also, this figure clearly shows that in the supersonic range, by varying the sweep angle, a preset static margin can be maintained at any Mach number. In order to demonstrate this, a +6% stable configuration with different wing planforms was considered. The three planforms consisted of; 1) the original planform with the front and the back wings having the same chord and span, 2) with wings of equal span but chord ratio of 1.5, and 3) with equal chords but front to back span ratio of 1.1. For supersonic flight, sweep schedule versus Mach number of these configurations is shown in Figure 20. It is quite evident in this figure that a constant static margin can be maintained over a range of flight Mach numbers through proper choice of the sweep angle.

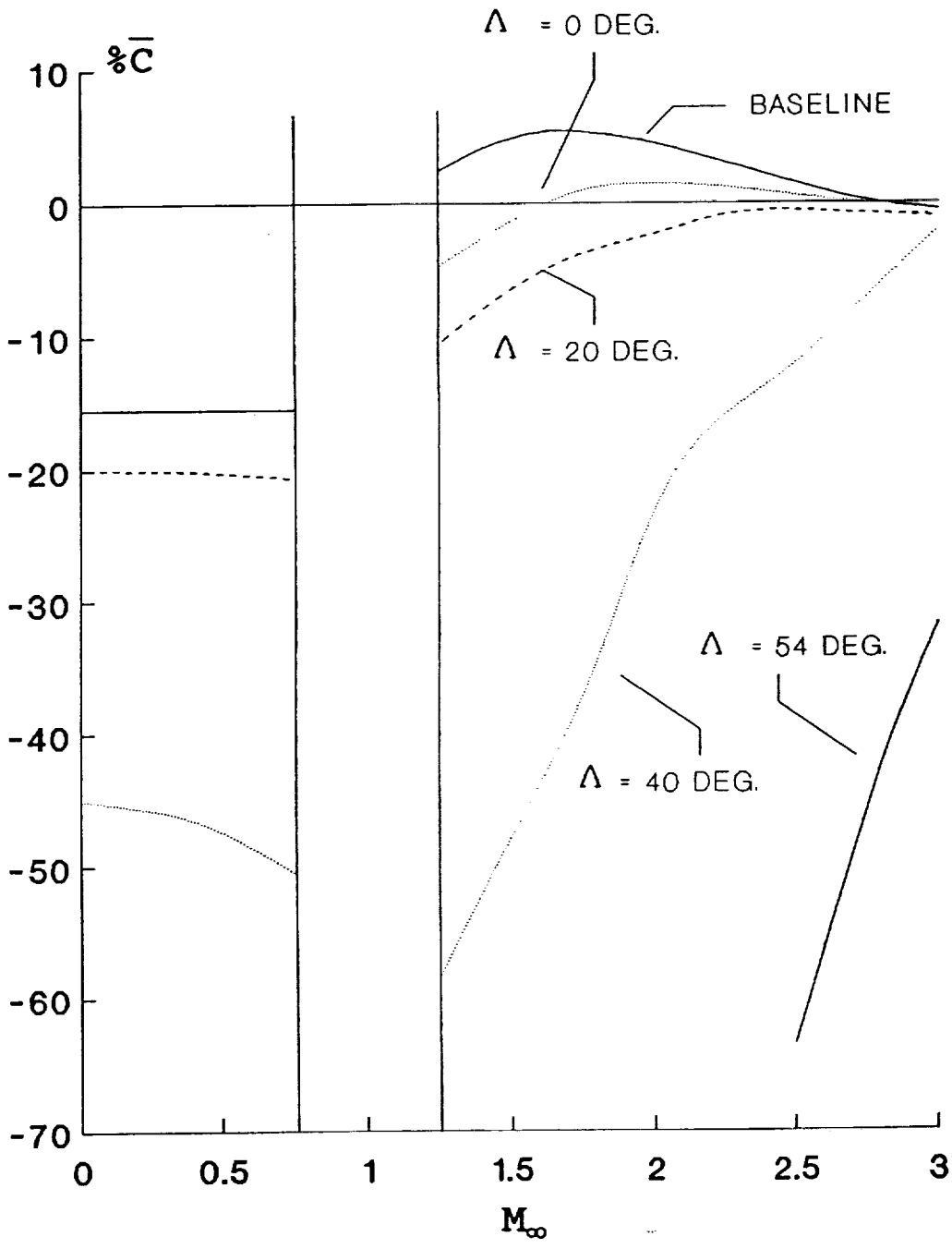

Figure 19. Static Margin.

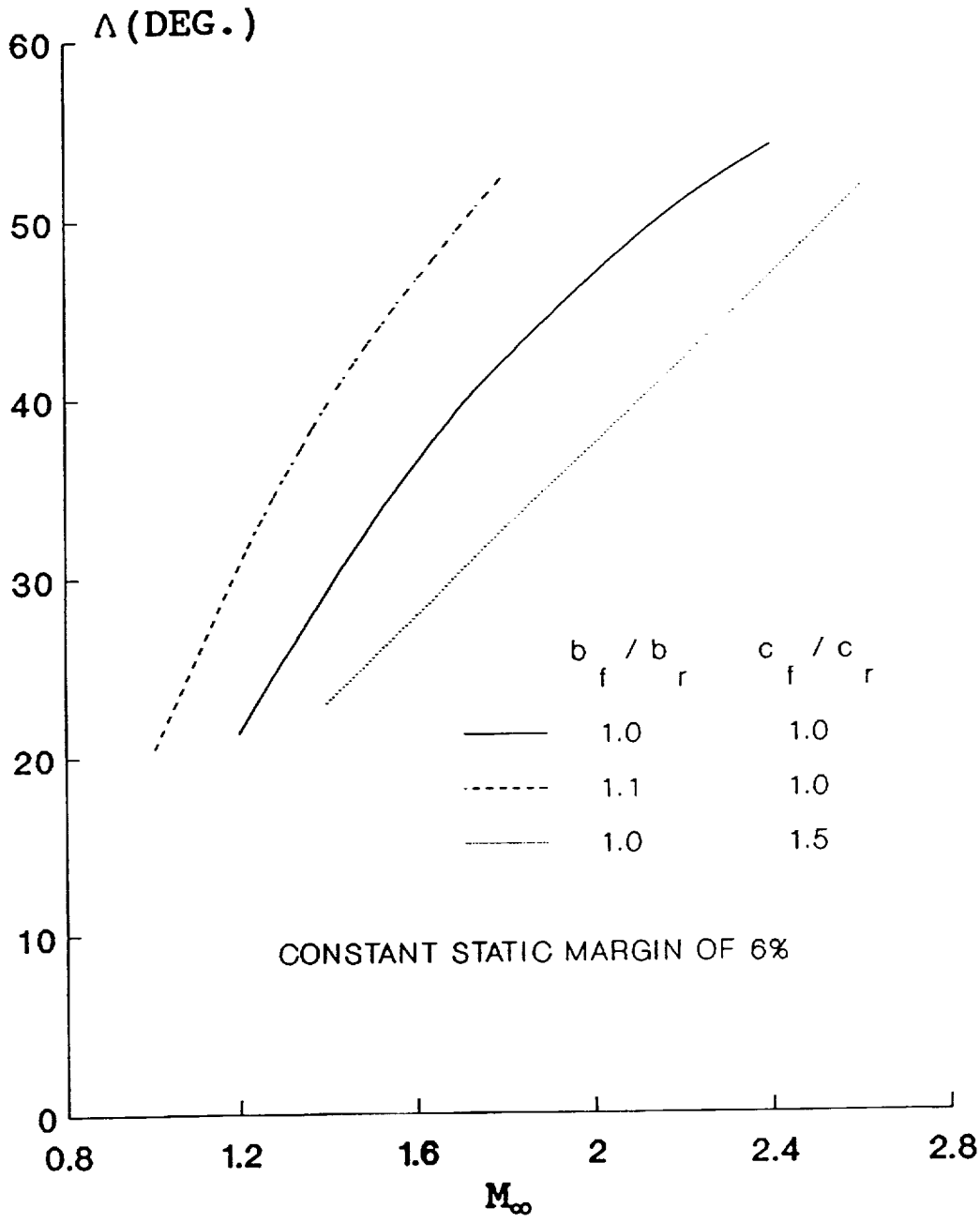

Figure 20. Sweep Schedule for Constant 6% Static Margin.

B. TRANSONIC FLIGHT

The program CANTATA was used to investigate the transonic aerodynamic characteristics of the scissor wing in comparison with the baseline. Since CANTATA was limited to two lifting surfaces, all configurations were considered without a stabilizer, and therefore untrimmed. Also, The scissor wings were modeled with a gap of approximately 25% of the chord because CANTATA would not run for smaller gaps.

Figure 21 shows the effect of decalage angle on the total lift to drag ratio. It is evident in this figure that decalage angle of negative 2 degrees represents the best compromise over the entire range of lift coefficients. This is consistent with the incompressible results presented in the previous section. The effect of this decalage angle becomes even more pronounced with increasing Mach number, as shown in Figures 22 and 23. In all these figures, the baseline has a higher maximum lift to drag ratio for lift coefficient of less than approximately 0.35. However, this range of lift coefficient corresponds only to transonic level flight at sea level. At Mach number of 0.8, the lift coefficient is about 0.22 at 15K ft and increases to 0.42 at 30K ft. Furthermore, during air combat, average lift coefficient is much greater due to increased load factor. At sea level, a 2g turn at Mach number of 0.8 requires a lift coefficient of 0.35. Due to these reasons, the apparent superiority of the base line at low lift coefficients is not utilized in actual flight.

Another advantage of a decalage of negative two degrees was

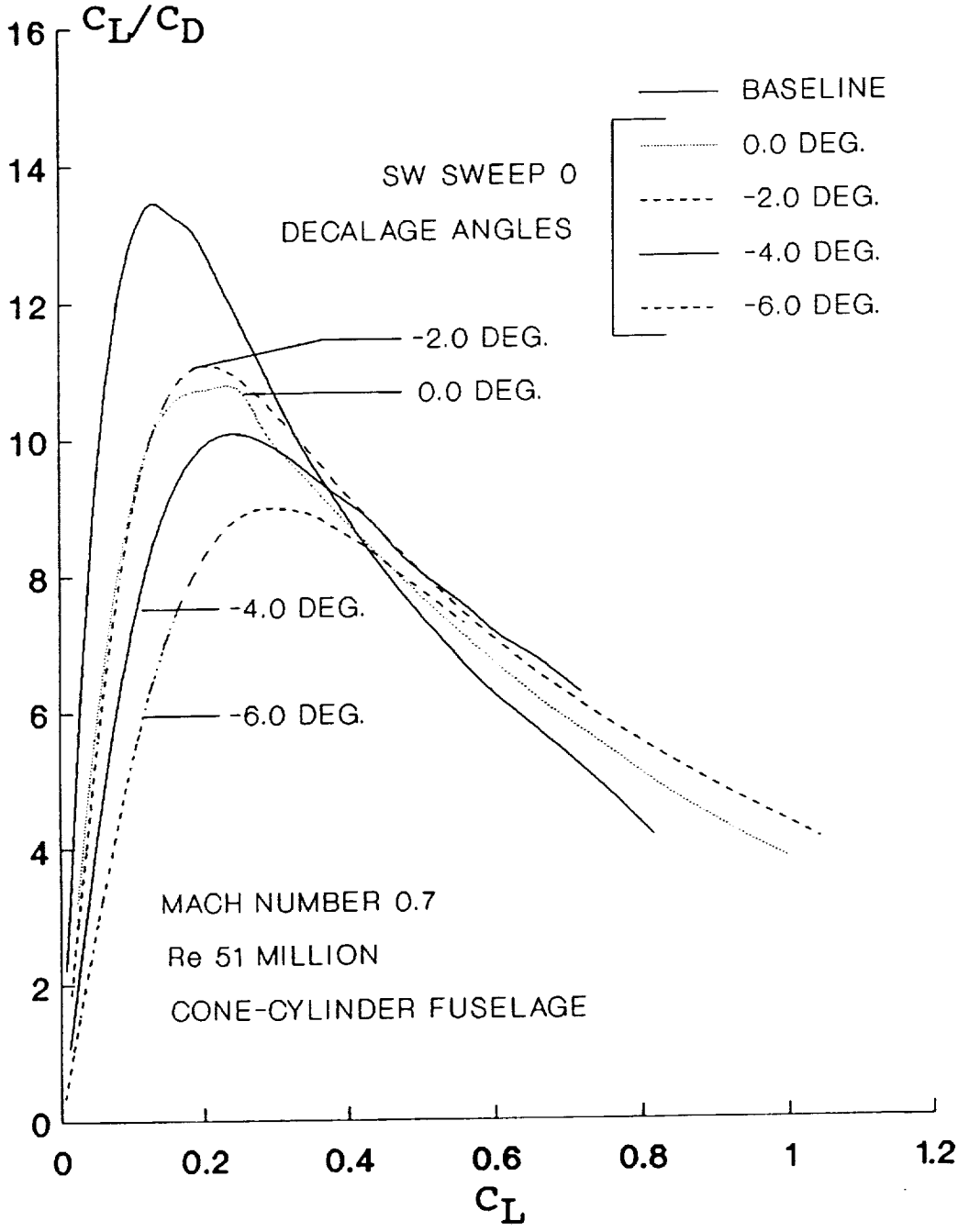

Figure 21. Effect of Decalage on Transonic Lift to Drag Ratio.

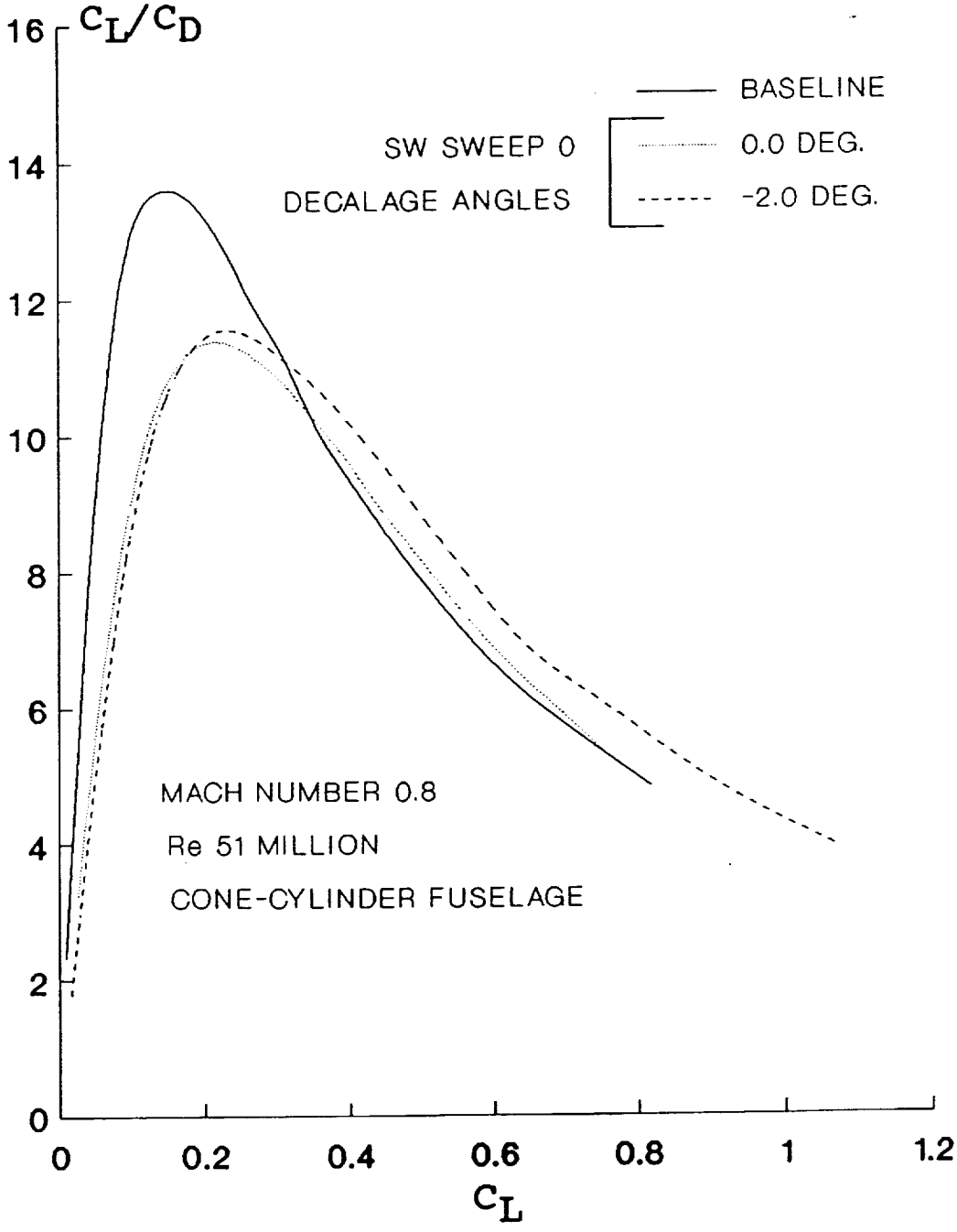

Figure 22. Lift to Drag Ratio at M_∞ = 0.8.

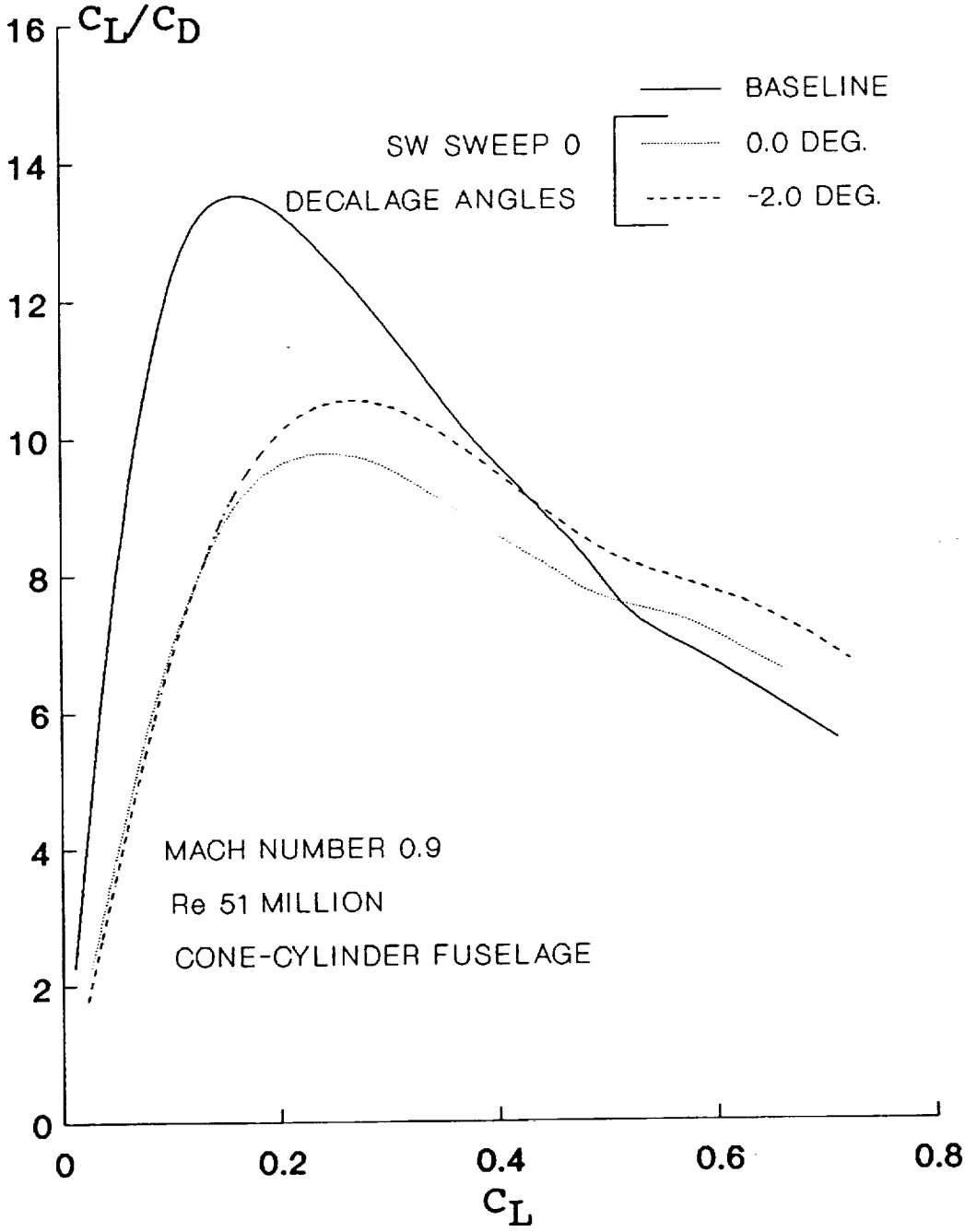

Figure 23. Lift to Drag Ratio at $M_\infty = 0.9$.

roughly equalizing the loads on both wings. Figure 24 shows the spanwise lift distribution for the same lift coefficient on the front and the back wings. This figure shows that without any decalage, the majority of the lift is produced by the front wing. Addition of a negative two degree decalage equalizes the loads. Of course, the required amount of decalage for this purpose increases with average lift coefficient. This is assumed to be obtainable through deflection of the leading edge flap on the front wing and the trailing edge flap on the rear wing.

In an attempt to bring the lift distributions closer to elliptic, the rear wing was also given a washout of 3 degrees. The resulting lift distribution is shown in Figure 25. In this case, for a clearer picture, the fuselage was omitted from the calculations. The resulting lift to drag ratio is also presented in Figure 26 for three sweep angles. It is assumed that the scissor wing configuration will not be flying in the transonic regime with no sweep because of the behavior of the pitching moment. It is evident from this figure that even the 20 degree sweep case compares well with the baseline.

One of the concerns in the transonic range was the behavior of the pitching moment in this regime. Figure 27 shows the variation of the pitching moment coefficient with lift coefficient at Mach number of 0.9. It is understood that the magnitude of the pitching moment coefficient is entirely dependent on the location of the moment center. Therefore, the magnitude of this parameter is of no importance. The important factor here is the change in the slope of these curves as lift coefficient changes.

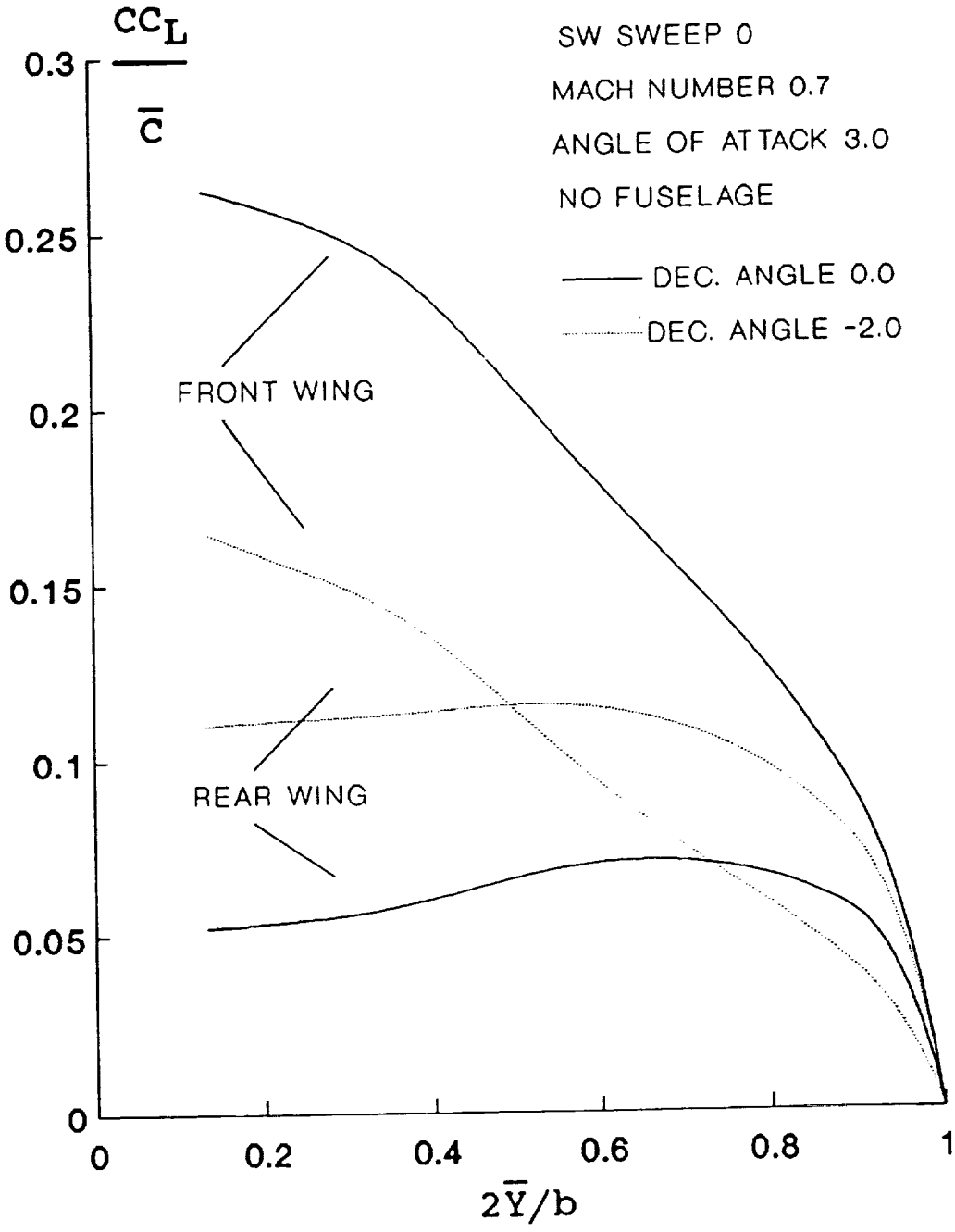

Figure 24. Effect of Decalage on Relative Lifts.

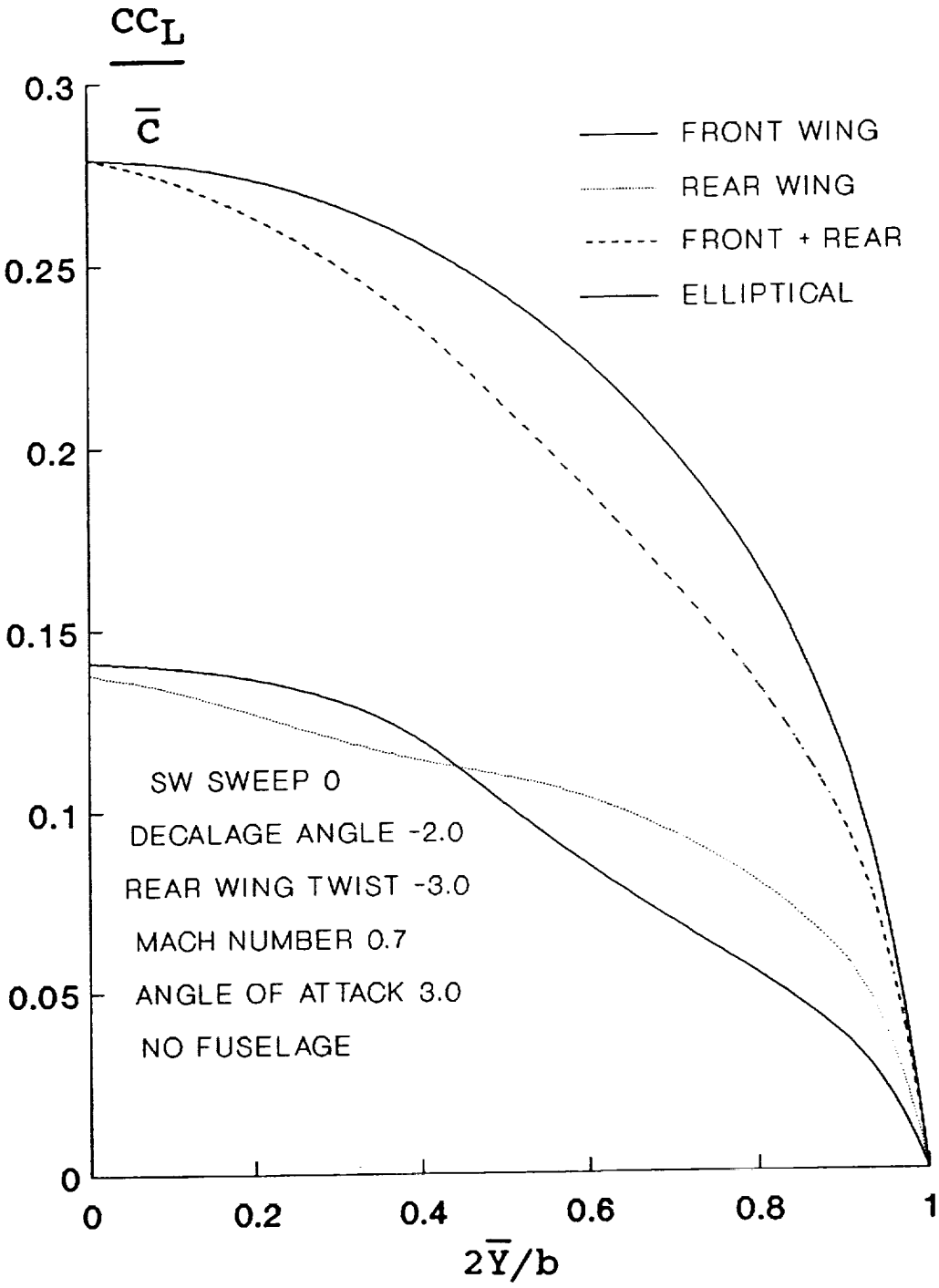

Figure 25. Effect of Twist on Spanwise Lift Distribution at $C_L = 0.25$.

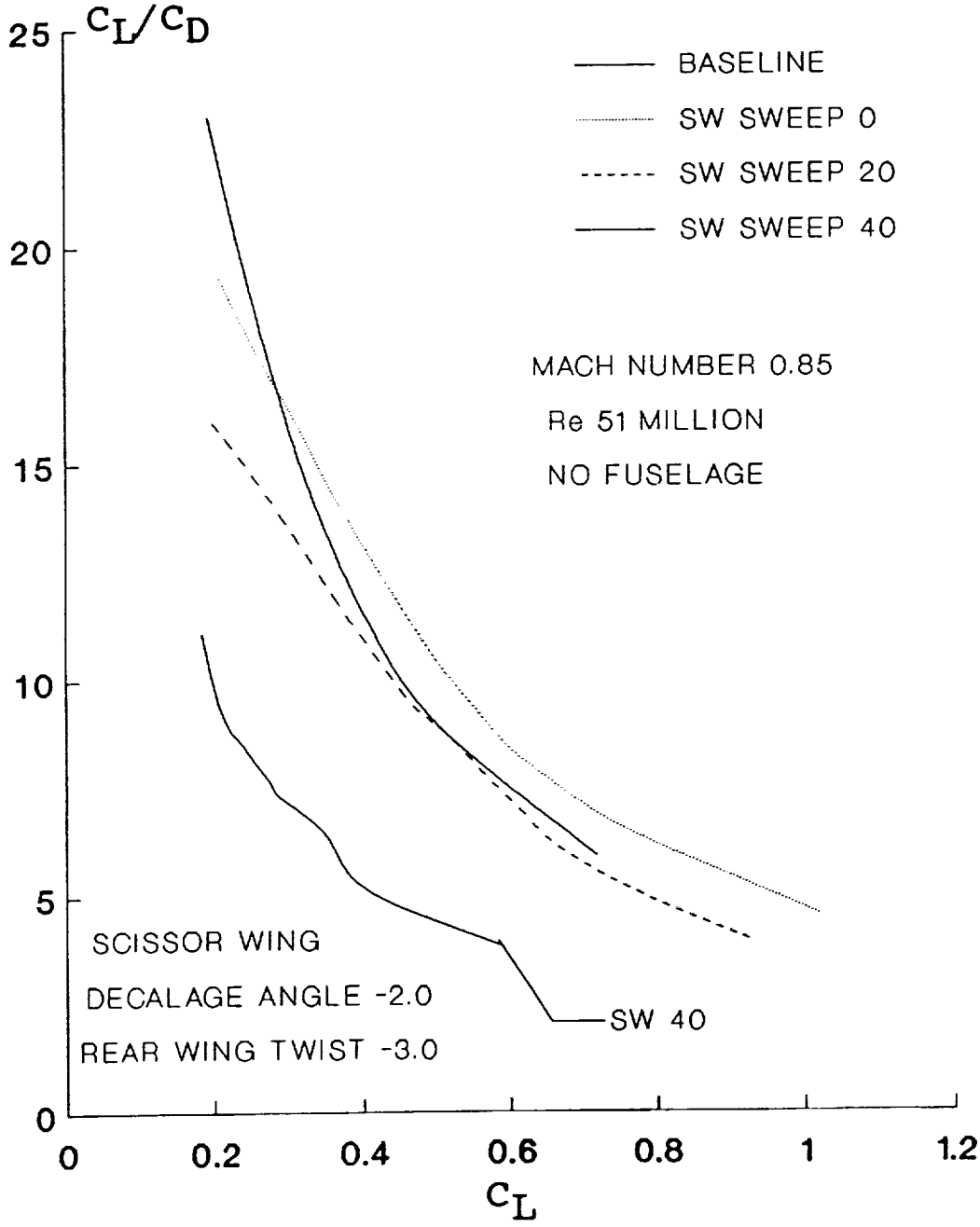

Figure 26. Lift to Drag Ratio for Combination of Washout and Decalage.

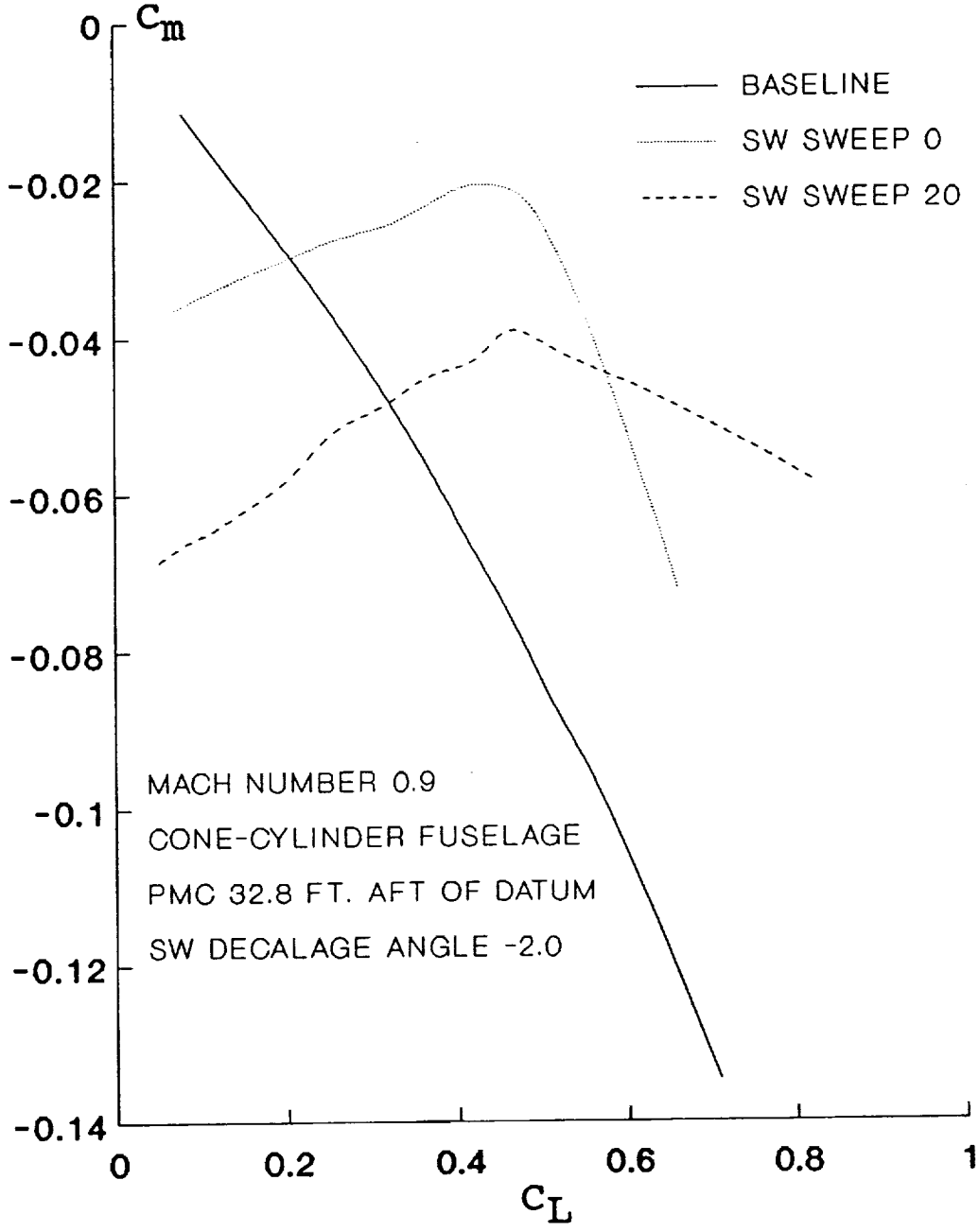

Figure 27. Pitching Moment Variation in Transonic Flow.

Large changes in the slope can result in the tendency of the aircraft to tuck under during certain maneuvers. The baseline with 23 degrees of leading edge sweep angle shows little change in slope compared with the scissor wing at zero sweep. However, it is also clear that the change in the slope of the scissor wing shown in this figure becomes less as the sweep angle increases to 20 degrees. This is consistent with the statement made in the previous paragraph regarding the choice of the sweep angle in the transonic region. Larger sweep angles could not be investigated due to convergence problems with CANTATA. The cause of these problems can be seen in the chordwise pressure distribution even at the sweep angle of 20 degrees in Figure 28. Tailoring of the airfoil shape can minimize of eliminate the strong shocks and hence moment slope changes shown in Figure 27.

Careful consideration of the results presented in this section reveals no unusual transonic behavior peculiar to the scissor wing compared with the baseline. Considering that the baseline was a nearly optimized configuration, it is felt that further transonic refinements can be made to render the scissor wing even better in this flight regime.

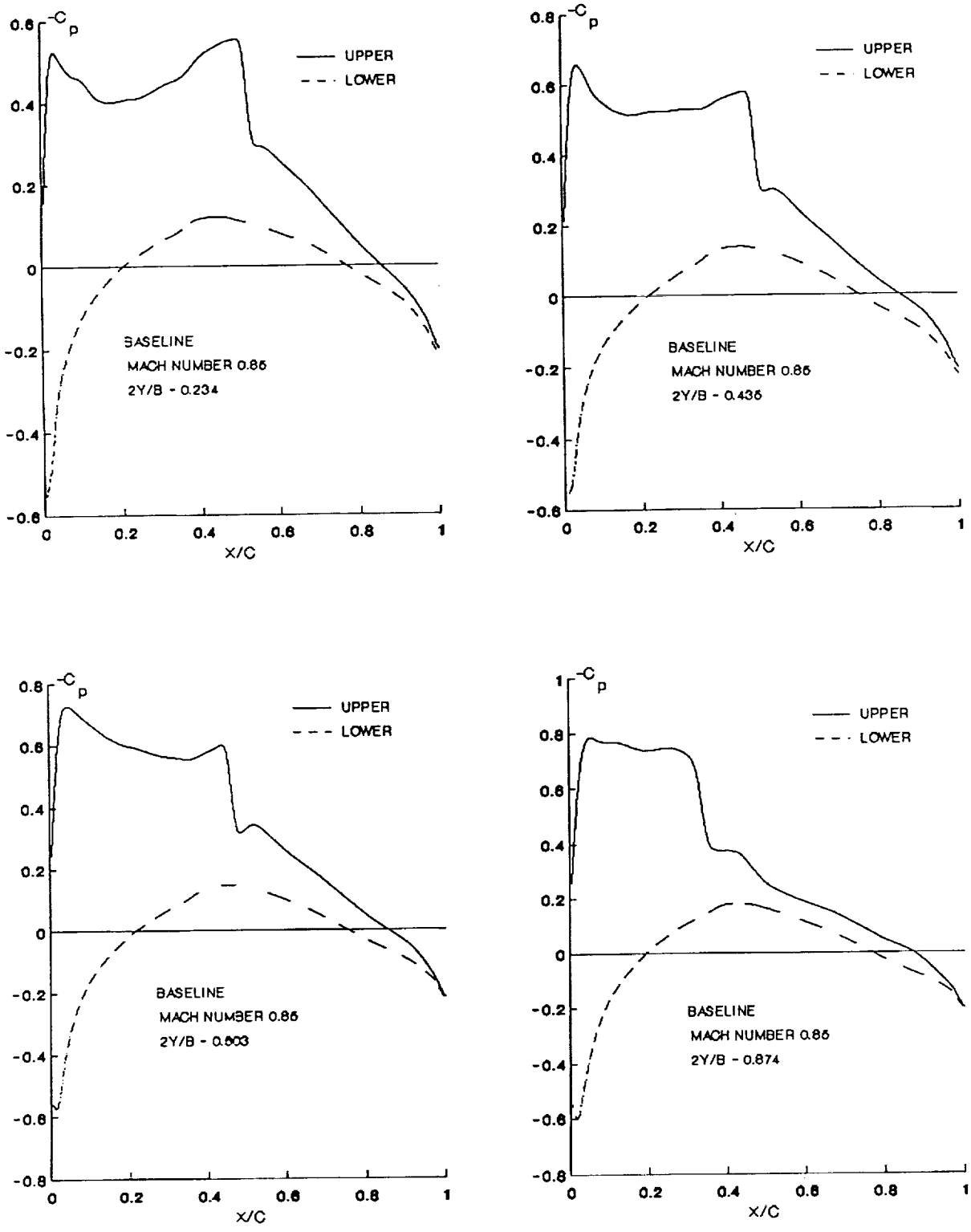

Figure 28-a. Spanwise Pressure Distribution of the Baseline, $C_L = 0.41$.

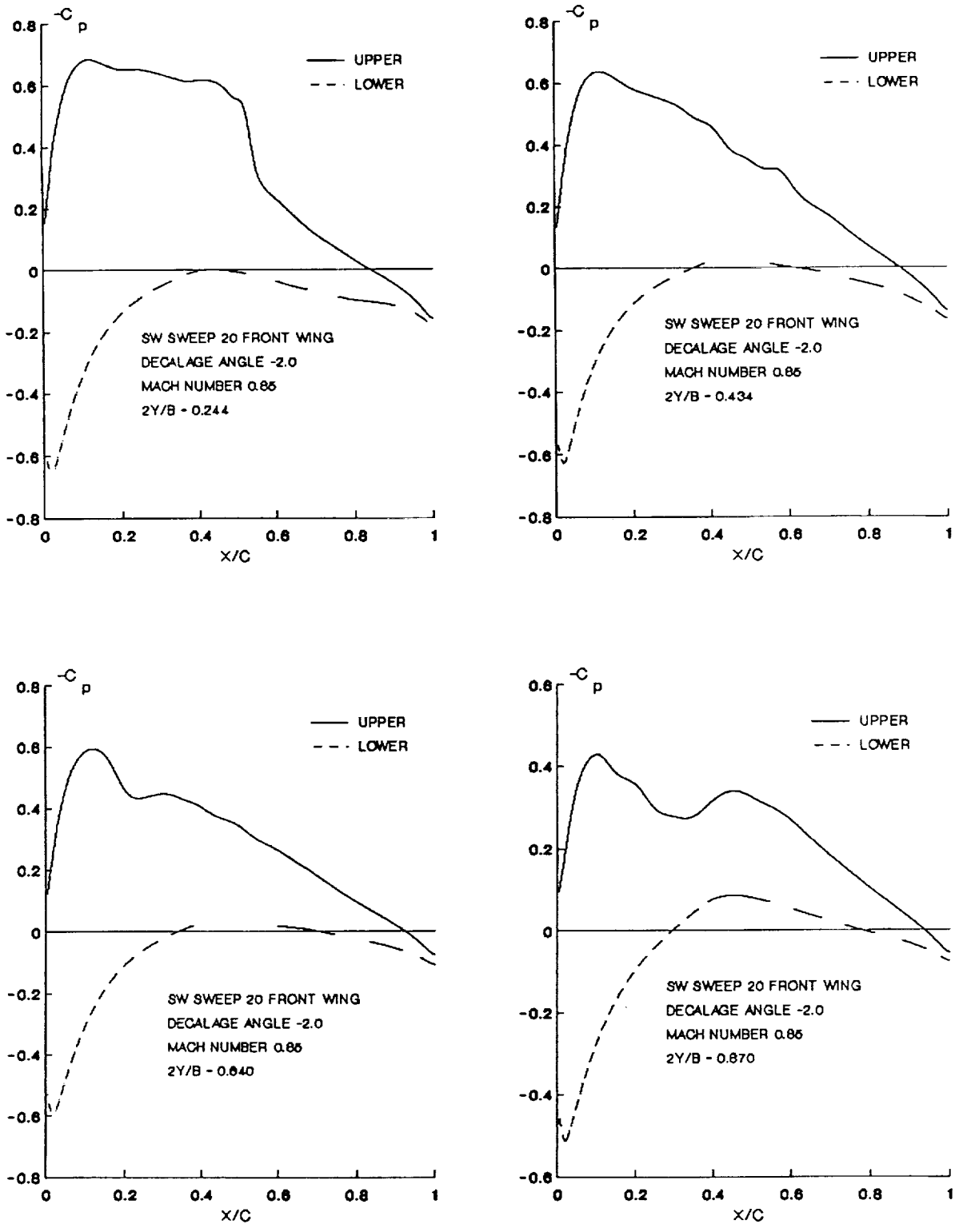

Figure 28-b. Spanwise Pressure Distribution on the Front Wing of the Scissor Wing at 20 Degree Sweep, $C_L = 0.20$.

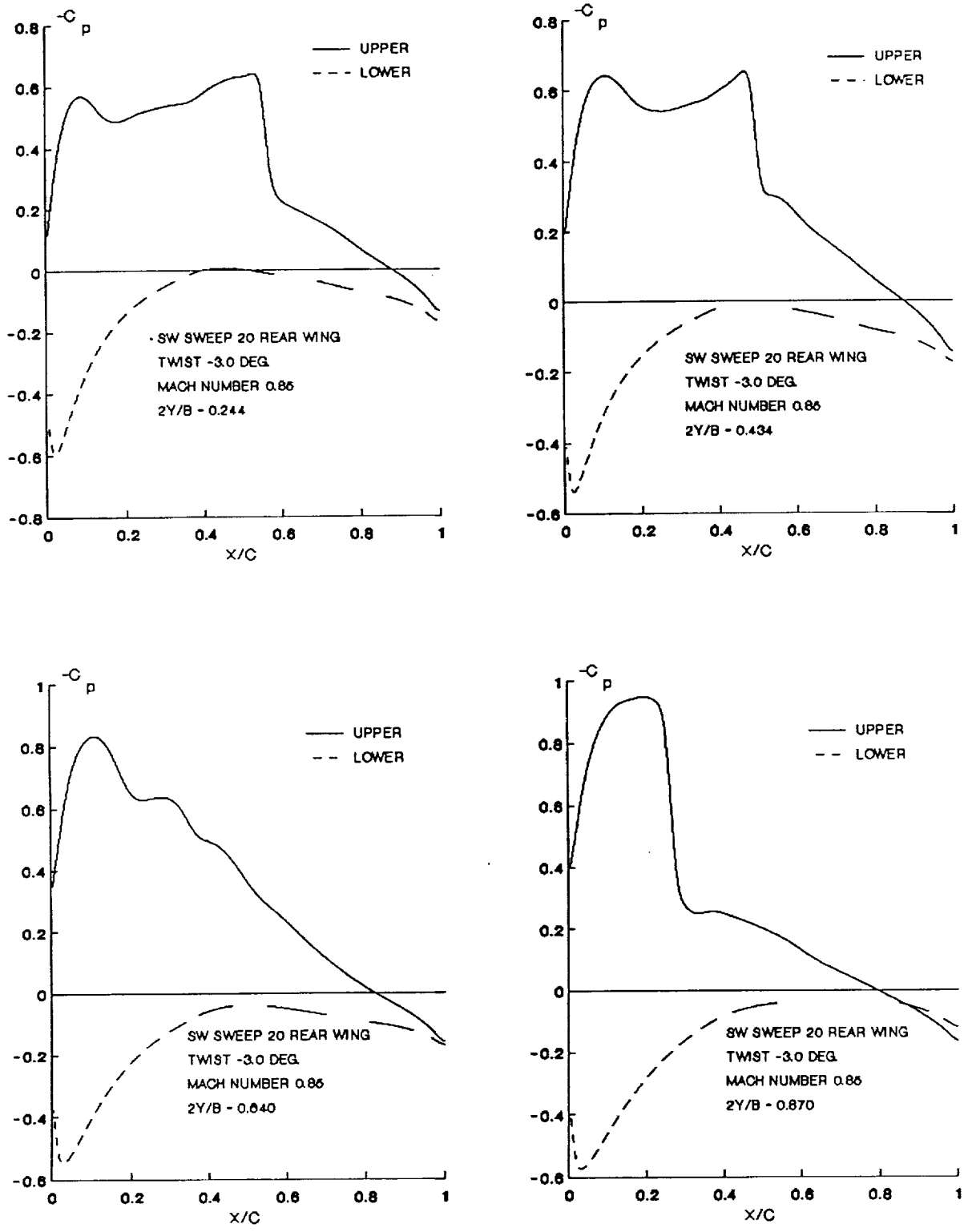

Figure 28-c. Spanwise Pressure Distribution on the Rear Wing of the Scissor Wing at 20 Degree Sweep, C_L = 0.21.

C. SUPERSONIC FLIGHT

In this flight regime the zero lift wave drag is the most dominant part. Therefore, the major research emphasis in the supersonic regime was placed on this parameter. Zero lift wave drag results for the six percent thickness NACA 64A-006 airfoil for the baseline and scissor wing configurations at sweep angles of 20, 40, and 54 degrees are shown in Figure 29. The 20 degree sweep scissor configurations wave drag is more than fifteen percent lower than the baseline for Mach numbers between 1.5 and 2.0. The 40 degree sweep scissor case has wave drag which is between 27 and 37 percent lower than the baseline for Mach numbers between 1.5 and 3.0. The 54 degree sweep scissor case has wave drag which is between 25 and 50 percent lower than the baseline for Mach numbers between 1.5 and 3.0. In all cases the scissor wing configuration offers substantial reductions in zero lift wave drag over the baseline configuration.

Wave drag was also investigated for a scissor wing canard configuration as shown in Figure 3f. A five percent stable canard configuration and a nine percent unstable canard were studied. Figure 30 illustrates the zero lift wave drag for the scissor-canard configuration at a 20 degree sweep angle in comparison with the 20 degree conventional scissor. The stable canard-scissor's wave drag is slightly higher than the conventional scissor while the unstable canard-scissor is slightly lower than the conventional scissor. However, the differences between all three configurations is small.

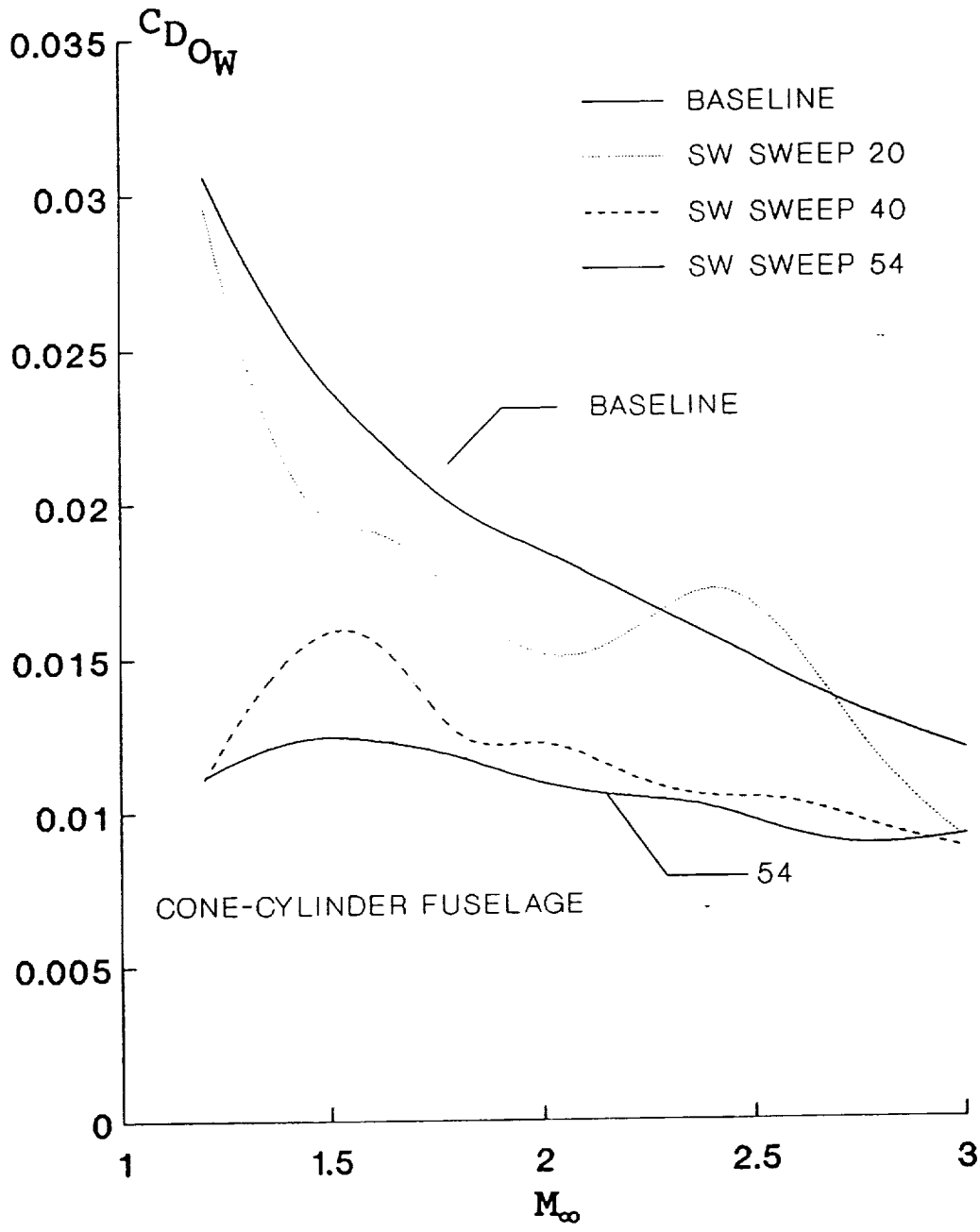

Figure 29. Zero Lift Wave Drag of the Baseline Compared with the Scissor Wing.

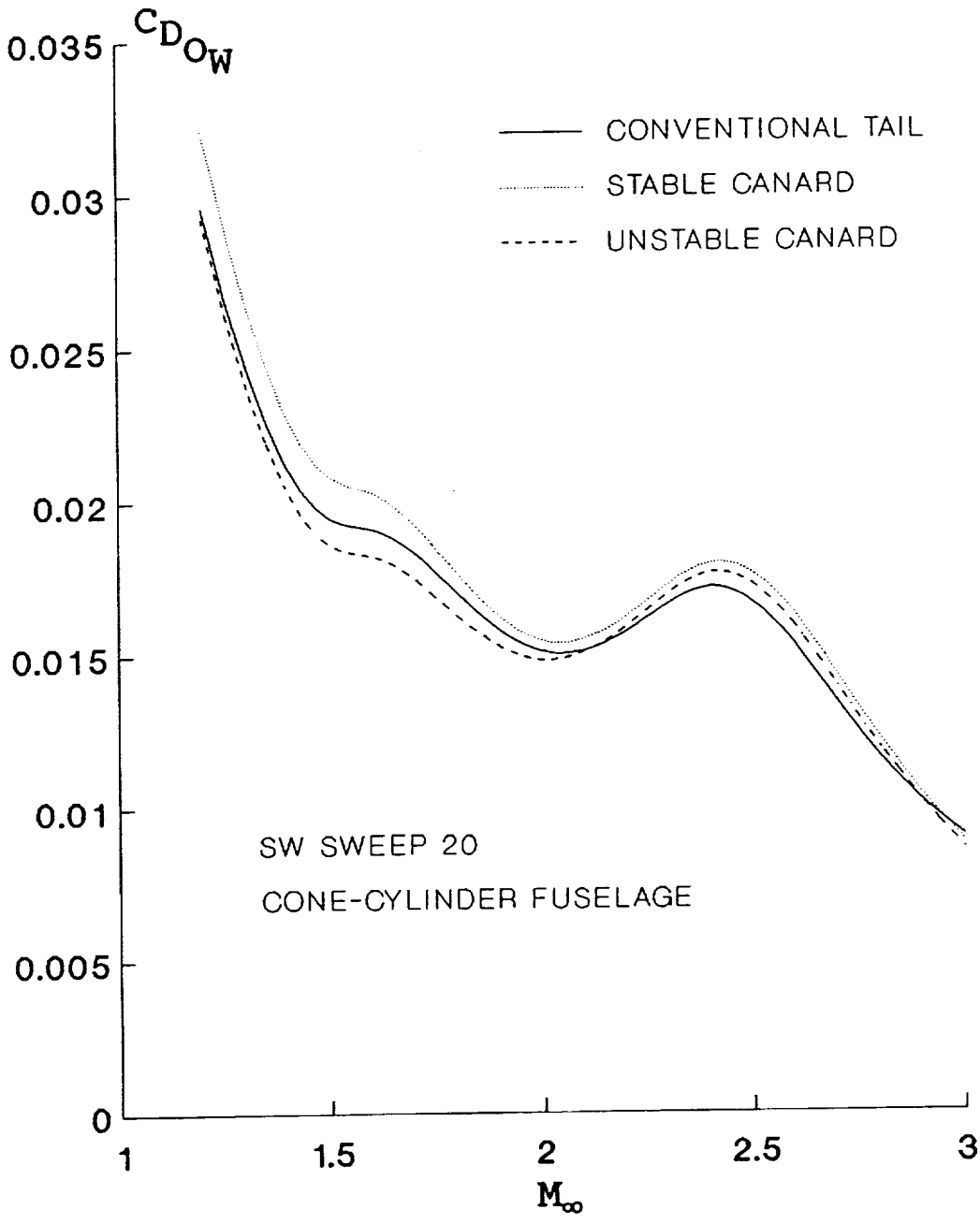

Figure 30. Zero Lift Wave Drag of Conventional and Canard Scissor Wings.

Fuselage wasting was investigated for both the scissor and the baseline. Fuselage wasting had negligible effect on the zero lift wave drag for the baseline but reduced the zero lift wave drag for the scissor configuration. The wave drag reduction is shown in Figure 31 and is of the order of 20 percent or more over the Mach number range from 1.5 to 3.0.

Finally, total configuration lift to drag ratio is presented in Figure 32. Here, the scissor wing at different sweep angles is compared with the baseline under trim at 30K ft altitude. In this case, component drag build hase been used to estimate total drag. In the supersonic range, the zero lift wave drag has also been included. Again, the viscous drag coefficient has been assumed to be constant. The superiority of the scissor wing with 54 degree sweep angle at higher Mach numbers is quite evident in this figure. Further estimates have shown that the difference in the lift to drag ratio between the baseline and the scissor wing can results in differences in the flight Mach numbers of as much as 0.25 for the same power.

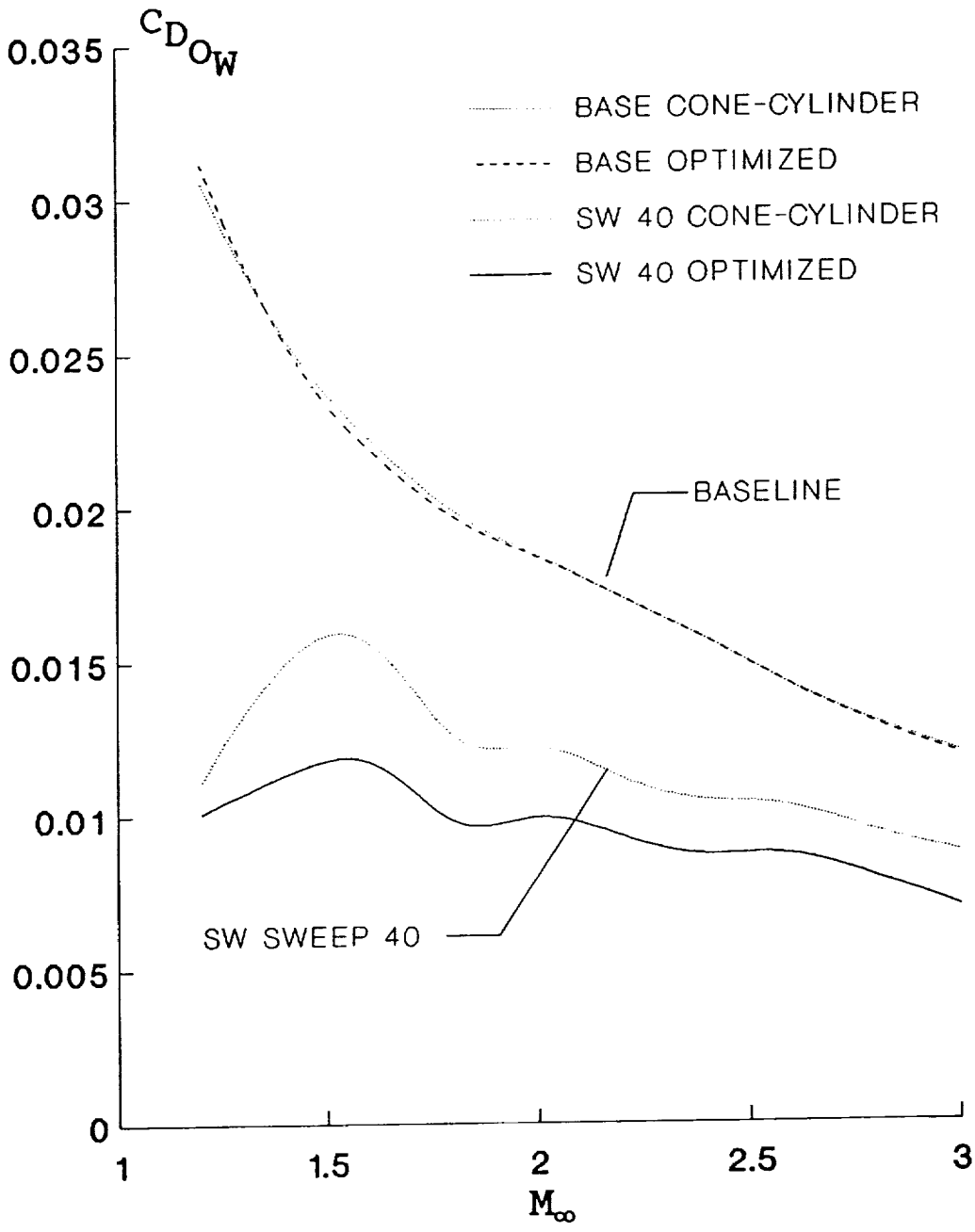

Figure 31. Effect of Fuselage Tapering on Zero Lift Wave Drag of the Baseline and the Scissor Wing.

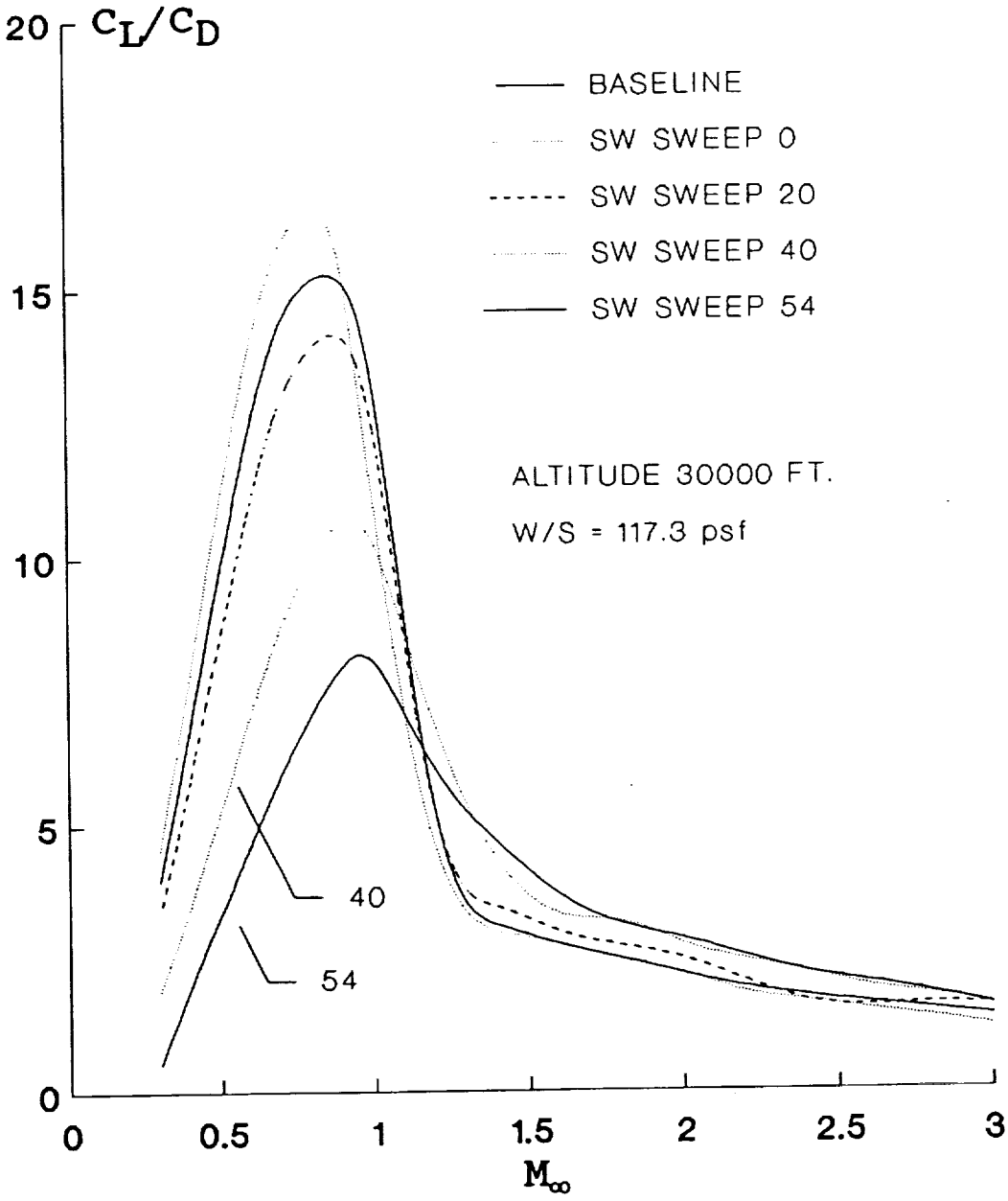

Figure 32. Total Configuration Lift to Drag Ratio.

CONCLUSIONS

A scissor wing configuration, consisting of two independently sweeping wings was numerically studied. This configuration was also compared with an equivalent fixed wing baseline. Aerodynamic and stability and control characteristics of these geometries were investigated over a wide range of flight Mach numbers.

It was demonstrated that in the purely subsonic flight regime, the scissor wing can achieve higher aerodynamic efficiency as the result of slightly higher aspect ratio. In the transonic regime, the lift to drag ratio of the scissor wing was shown to be higher than that of the baseline, for higher values of the lift coefficient. This suggested that the scissor wing would be more efficient during transonic cruise at high altitudes as well as during air combat at all altitudes. In supersonic flight, where the wings are maintained at maximum sweep angle, the scissor wing was shown to have a decided advantage in terms of reduced wave drag.

From the view point of stability and control, the scissor wing was shown to have distinct advantages. It was shown that this geometry can maintain a constant static margin in supersonic as well as subsonic flight, by proper sweep scheduling. Furthermore, it was demonstrated that addition of wing mounted elevons can greatly enhance control authority in pitch and roll.

REFERENCES

1. "The Anals of Polymorph, A Short History of V-G," Air International, Vol. 8, No. 3, 1975.
2. Polhamus, E. C. and Toll, T. A., "Research Related to Variable Sweep Aircraft Development," NASA TM-83121, 1981.
3. Alford, W. J. and Polhamus, E. C., "Variable Sweep Wing Configuration," United States Patent #3053484, 1962.
4. Jones, R. T., "Obliques Wing Supersonic Aircraft," United States Patent #3971535, 1976.
5. Rokhsaz, K., "Scissor Wing Patent Disclosure," Disclosure #87-UMR-023, 1986.
6. Rokhsaz, K. and Selberg, B. P., "Static Stability and Control Characteristics of Scissor Wing Configurations," Journal of Aircraft, Vol. 27, No. 4, 1990.
7. Tulinius, J., "Unified Subsonic, Transonic, and Supersonic NAR Vortex Lattice," North American Rockwell, TFD-72-523, 1972.
8. Lan, E. C. and Chang, J. F., "Calculation of Vortex Lift Effect for Cambered Wings by the Suction Analogy," NASA CR-3449, 1981.
9. Nicolai, L. M., Fundamentals of Aircraft Design, METS Inc., San Jose, CA, 1975.
10. Craidon, C. B., "User's Guide for a Computer Program for Calculating the Zero-Lift Wave Drag of Complex Configurations," NASA TM-85670, 1984.

11. Boppe, C. W., "Transonic Flowfield Analysis for Wing-Fuselage Combinations," NASA CR-3243, 1980.

12. Aidala, P., "Numerical Aircraft Design Using 3-D Transonic Analysis with Optimization," AFWAL-TR-3091, 1981.

13. Stevens, W. A., Goradia, S. H., and Braden, J. A., "Mathematical Model for Two-Dimensional Muti-Component Airfoils in Viscous Flow, NASA CR-1843, 1971.